



# Pt-Assisted Carbon Remediation of Mo<sub>2</sub>C Materials for CO Disproportionation

March 2020

*Changing the World's Energy Future*

Zongtang Fang, Lucun Wang, Yixiao Wang, Rebecca R Fushimi



**DISCLAIMER**

This information was prepared as an account of work sponsored by an agency of the U.S. Government. Neither the U.S. Government nor any agency thereof, nor any of their employees, makes any warranty, expressed or implied, or assumes any legal liability or responsibility for the accuracy, completeness, or usefulness, of any information, apparatus, product, or process disclosed, or represents that its use would not infringe privately owned rights. References herein to any specific commercial product, process, or service by trade name, trade mark, manufacturer, or otherwise, does not necessarily constitute or imply its endorsement, recommendation, or favoring by the U.S. Government or any agency thereof. The views and opinions of authors expressed herein do not necessarily state or reflect those of the U.S. Government or any agency thereof.

# **Pt-Assisted Carbon Remediation of Mo<sub>2</sub>C Materials for CO Disproportionation**

**Zongtang Fang, Lucun Wang, Yixiao Wang, Rebecca R Fushimi**

**March 2020**

**Idaho National Laboratory  
Idaho Falls, Idaho 83415**

**<http://www.inl.gov>**

**Prepared for the  
U.S. Department of Energy  
Under DOE Idaho Operations Office  
Contract DE-AC07-05ID14517, DE-AC07-05ID14517**

## Pt-Assisted Carbon Remediation of Mo<sub>2</sub>C Materials for CO Disproportionation

Zongtang Fang, Lu-Cun Wang, Yixiao Wang, Ember Sikorski, Shuai Tan, Katie Dongmei Li-Oakey, Lan Li, Gregory Yablonsky, David A Dixon, and Rebecca R. Fushimi  
*ACS Catal.*, **Just Accepted Manuscript** • DOI: 10.1021/acscatal.9b05225 • Publication Date (Web): 06 Jan 2020

Downloaded from [pubs.acs.org](https://pubs.acs.org) on January 11, 2020

### Just Accepted

“Just Accepted” manuscripts have been peer-reviewed and accepted for publication. They are posted online prior to technical editing, formatting for publication and author proofing. The American Chemical Society provides “Just Accepted” as a service to the research community to expedite the dissemination of scientific material as soon as possible after acceptance. “Just Accepted” manuscripts appear in full in PDF format accompanied by an HTML abstract. “Just Accepted” manuscripts have been fully peer reviewed, but should not be considered the official version of record. They are citable by the Digital Object Identifier (DOI®). “Just Accepted” is an optional service offered to authors. Therefore, the “Just Accepted” Web site may not include all articles that will be published in the journal. After a manuscript is technically edited and formatted, it will be removed from the “Just Accepted” Web site and published as an ASAP article. Note that technical editing may introduce minor changes to the manuscript text and/or graphics which could affect content, and all legal disclaimers and ethical guidelines that apply to the journal pertain. ACS cannot be held responsible for errors or consequences arising from the use of information contained in these “Just Accepted” manuscripts.

## Pt-Assisted Carbon Remediation of Mo<sub>2</sub>C Materials for CO Disproportionation

Zongtang Fang,<sup>a</sup> LuCun Wang,<sup>a</sup> Yixiao Wang,<sup>a</sup> Ember Sikorski,<sup>b,c</sup> Shuai Tan,<sup>c,d</sup> Dongmei  
(Katie) Li-Oakey,<sup>c,d</sup> Lan (Samantha) Li,<sup>b,c</sup> Gregory Yablonsky,<sup>e</sup> David A. Dixon<sup>f</sup>, Rebecca  
Fushimi<sup>a,\*</sup>

<sup>a</sup> Biological and Chemical Science and Technology, Idaho National Laboratory, Idaho Falls, ID  
83401

<sup>b</sup> Micron School of Materials Science and Engineering, Boise State University, Boise, ID 83725

<sup>c</sup> Center for Advanced Energy Studies, Idaho Falls, ID 83401

<sup>d</sup> Department of Chemical Engineering, University of Wyoming, Laramie, WY 82071

<sup>e</sup> Department of Energy, Environment and Chemical Engineering, Washington University in  
Saint Louis, Saint Louis, MO 63103

<sup>f</sup> Department of Chemistry, The University of Alabama, Tuscaloosa, AL 35487-0336

### Abstract

Using the CO disproportionation (Boudouard) reaction as a probe reaction, an in-depth analysis of temperature-programmed pulse response data shows that the addition of Pt to Mo<sub>2</sub>C mitigates deactivation of Mo active sites by acting as a carbon collector. CO<sub>2</sub> production on Mo<sub>2</sub>C and Pt/Mo<sub>2</sub>C materials is dependent on both the activation energy and the CO surface concentration.

---

\* Corresponding authors: rebecca.fushimi@inl.gov, dadixon@ua.edu

1  
2  
3 Detailed plane-wave density functional theory calculations of the CO adsorption and disproportion  
4 reactions on Mo<sub>2</sub>C supported Pt nanoparticles (NPs) are reported. The Mo<sub>2</sub>C was modeled by the  
5  
6  $\beta$ -Mo<sub>2</sub>C (100) surface and the Pt/Mo<sub>2</sub>C interface was modeled by the addition of 12 Pt atoms to  
7  
8 the Mo<sub>2</sub>C (100) surface (12Pt@Mo<sub>2</sub>C). The potential energy surfaces of the Boudouard reaction  
9  
10 were calculated on pure Mo<sub>2</sub>C, 12Pt@Mo<sub>2</sub>C as well as Pt (111) surfaces. CO dissociation readily  
11  
12 occurs on the Mo<sub>2</sub>C (100) surface, but not on the Pt (111) surface with the former being exothermic  
13  
14 and the latter being endothermic. At the Pt/Mo<sub>2</sub>C interface, CO dissociation is still exothermic,  
15  
16 but with a larger energy barrier. The Boudouard reaction takes place on the Mo<sub>2</sub>C region where  
17  
18 CO<sub>2</sub> is formed from a surface O atom dissociated from one CO molecule in reaction with another  
19  
20 CO molecule leaving one C atom on the surface. C adsorption is preferential on the Pt site in  
21  
22 comparison to the Mo site. The supported Pt domains can collect remaining C atoms, facilitating  
23  
24 further CO<sub>2</sub> formation on the active Mo sites. A Bader charge analysis shows that the surface  
25  
26 metal-carbon bond is a mixture of covalent and ionic bonds whereas the surface metal-oxygen  
27  
28 bond is ionic. Electron localization function (ELF) and partial charge density calculations agree  
29  
30 well with the Bader charge analysis. These computational results are consistent with experimental  
31  
32 observations of the interaction of CO with Mo<sub>2</sub>C-nanotube supported Pt-domains in the transient  
33  
34 regime under far-from equilibrium conditions. The Boudouard reaction is an important side  
35  
36 reaction and the unexpected role found for Pt as a carbon collector, with Mo serving as a  
37  
38 disproportionation site, provides a unique vantage point for understanding carbon and coke  
39  
40 formation on catalytic materials.  
41  
42  
43  
44  
45  
46  
47  
48  
49  
50  
51  
52  
53  
54  
55  
56  
57  
58  
59  
60

## Introduction

The adsorption and reaction processes of CO on transition-metal surfaces have been the subject of studies for decades, because they are key steps in many catalytic processes, such as CO oxidation, the water-gas shift (WGS) reaction,<sup>1</sup> CO methanation,<sup>2</sup> and Fischer-Tropsch synthesis.<sup>3</sup> Despite extensive research efforts, there are still many open questions regarding the reaction mechanisms and active sites. It is known that the reactivity of CO depends critically on the electronic and geometric nature of the underlying metal surfaces. For instance, CO can readily decompose on Mo surfaces<sup>4</sup> whereas dissociative adsorption of CO on Pt surfaces may only occur under high temperature and pressure conditions.<sup>5</sup> Compared with the well-defined single crystal surfaces, the reaction mechanisms and active sites for CO activation are even more complex when transition metals are in the form of nanoparticles, which are usually dispersed on materials with high surface areas.

Transition metal carbides (TMCs), such as molybdenum carbide ( $\text{Mo}_2\text{C}$ ), have been reported to exhibit excellent catalytic properties in many reactions including  $\text{CO}_2$  reduction,<sup>6</sup>  $\text{CO}_2$  hydrogenation reactions,<sup>7,8</sup> CO hydrogenation,<sup>9</sup> and the WGS reaction<sup>10,11</sup> etc. For the WGS reaction on Pt/ $\text{Mo}_2\text{C}$  the reaction rate is significantly higher than the most active oxide-supported Pt catalysts, such as Pt/ $\text{CeO}_2$  and Pt/ $\text{TiO}_2$ <sup>12</sup>. In addition, it was shown that the reaction rate of the supported catalysts could be enhanced by a factor of 4-5 as compared to unsupported  $\text{Mo}_2\text{C}$ .<sup>12,13</sup> Atomic layered Au clusters on  $\alpha$ - $\text{MoC}$  are active to convert CO through the WGS process at a low temperature of 150 °C. <sup>14</sup> Highly dispersed copper over hexagonal  $\beta$ - $\text{Mo}_2\text{C}$  has been reported to be an efficient and stable catalyst for the reverse water gas shift reaction.<sup>15</sup> Other early transition metal carbides such as TM = Ti, Zr, Hf, V, Nb, Ta have been reported to be promising materials

1  
2  
3 for CO<sub>2</sub> activation as well as hydrogenation of CO<sub>2</sub>.<sup>16,17,18,19,20</sup> The reaction mechanisms and  
4  
5 origin of the synergistic effect, however, are still not fully addressed.  
6

7  
8 The interaction of CO with various Mo<sub>2</sub>C materials has been widely investigated with the  
9  
10 density functional theory.<sup>21,22,23,24,25,26</sup> Wang and Jiao studied the effect of coverage of CO  
11  
12 adsorption and dissociation on the orthorhombic Mo<sub>2</sub>C (100) surface and found that the  
13  
14 dissociative chemisorption is favorable for up to ½ monolayer of CO on the Mo terminated surface.  
15  
16  
17  
18 <sup>21,22</sup> In addition, they found that the most stable surface of hexagonal β-Mo<sub>2</sub>C changes as  
19  
20 temperature increases and is also dependent on the surrounding gas compositions.<sup>23</sup> The doping of  
21  
22 K has been reported to be favorable for CO molecular adsorption on a hexagonal β-Mo<sub>2</sub>C (001)  
23  
24 surface.<sup>24</sup> Li, et al found that the Ni doping can change the most favorable site for C adsorption  
25  
26 from the hollow Mo site to the Ni-Mo interface on the hexagonal β-Mo<sub>2</sub>C (001) surface.<sup>25</sup>  
27  
28 However, the best site for O adsorption remains unchanged.  
29

30  
31 Among various approaches to study catalytic reactions, the Temporal Analysis of Products  
32  
33 (TAP) probe molecule pulse response technique is particularly useful in extracting kinetic  
34  
35 information for the development of detailed reaction mechanisms for catalytic reactions on  
36  
37 complex materials.<sup>27,28</sup> TAP provides a unique experimental regime, far-from equilibrium, in  
38  
39 which industrial materials can be incrementally titrated with nanomole precision and millisecond  
40  
41 time resolution. The evolution of kinetic properties from TAP data shows how processes, such as  
42  
43 surface diffusion, number of active sites, reaction products, and effects of surface intermediates  
44  
45 and products impact the reaction mechanism. By removing the material from the process setting,  
46  
47 these detailed kinetic tests can be used to better understand at a fundamental level how/why one  
48  
49 material functions differently than another.  
50  
51  
52  
53  
54  
55  
56  
57  
58  
59  
60

1  
2  
3 In previous work by our group,<sup>10</sup> Pt/Mo<sub>2</sub>C materials were interrogated to understand  
4 electronic structure changes and CO bonds strengths using DRIFTS. Transient kinetic pulse  
5 response experiments in a TAP reactor were a smaller component of previous work to characterize  
6 CO adsorption, reaction pathways, and active sites in Mo<sub>2</sub>C nanotube supported Pt nanoparticles  
7 prepared by atomic layer deposition (ALD). Temperature programmed experiments were  
8 conducted in a continuous CO pulsing mode to investigate CO adsorption capacity and reactivities  
9 on both Pt/Mo<sub>2</sub>C and pure Mo<sub>2</sub>C catalysts. Significant CO<sub>2</sub> was produced on both pure Mo<sub>2</sub>C and  
10 Pt/Mo<sub>2</sub>C surfaces with the maximum production at higher temperature for Pt/Mo<sub>2</sub>C than that for  
11 pure Mo<sub>2</sub>C. It was concluded that CO<sub>2</sub> formation occurs via the process of CO disproportionation  
12 (forward Boudouard reaction,  $2\text{CO} \rightarrow \text{CO}_2 + \text{C}$ ) and that C atoms accumulate on the surface.  
13  
14  
15  
16  
17  
18  
19  
20  
21  
22  
23  
24  
25

26 Herein, we provide greater focus on the mechanism for accumulation of carbon atoms and  
27 the role of platinum in assisting this process using density functional theory (DFT) to better  
28 understand the original TAP results. It is important to note that the TAP transient low-temperature  
29 CO<sub>2</sub> production is not likely to be observed under steady-state flow conditions since the time scale  
30 and sensitivity of typical detection systems (e.g. GC-MS) far exceed this rate of change and the  
31 total amounts of CO<sub>2</sub> produced are extremely low. The distinctive transient measurement setting  
32 is used as a precise method for comparing the fundamental kinetic features of these materials and  
33 hence a greater level of detail for comparison to DFT results. Nonetheless, it provides no direct  
34 structural information about the active center for the Boudouard reaction, the Pt domain and  
35 interface. To close the structure-kinetics gap we can rely on DFT electronic structure calculations  
36 to better understand the surfaces responsible for our experimental kinetic observations.  
37  
38  
39  
40  
41  
42  
43  
44  
45  
46  
47  
48  
49  
50

51 This work combines both experimental techniques including TAP and transmission electron  
52 microscopy (TEM) characterizations with periodic DFT to identify the active sites for CO  
53  
54  
55  
56  
57

1  
2  
3 adsorption and disproportionation as well as the role of Pt nanoparticles in acting as a carbon  
4 collector. The catalysts were characterized by TEM after TAP experiments to investigate the  
5 structural change including carbon deposition. Previous work showed XRD patterns of Mo<sub>2</sub>C  
6 nanotubes corresponding to the pure hexagonal phase of Mo<sub>2</sub>C ( $\beta$ -Mo<sub>2</sub>C).<sup>29</sup> There is no uniform  
7 definition of different phases of Mo<sub>2</sub>C as well. We have noticed that the hexagonal and  
8 orthorhombic phases are called  $\alpha$ -Mo<sub>2</sub>C and  $\beta$ -Mo<sub>2</sub>C respectively by some researchers.<sup>16,17,21</sup> To  
9 be consistent with our previous work as well as some other experimental studies,<sup>10,29,30</sup> we use  $\beta$ -  
10 Mo<sub>2</sub>C for the HCP phase in this work. The  $\beta$ -Mo<sub>2</sub>C (100) surface was selected for the DFT  
11 calculations to model the CO adsorption and disproportionation reactions on a Mo<sub>2</sub>C nanotube as  
12 the lattice fringes of the Mo<sub>2</sub>C nanotube were in the direction of  $\beta$ -Mo<sub>2</sub>C (100) plane from an  
13 HRTEM image.<sup>29</sup> We studied the potential energy surface of the Boudouard reaction on both a  
14 pure  $\beta$ -Mo<sub>2</sub>C (100) surface and a Pt/Mo<sub>2</sub>C interface. The Boudouard reaction on Pt (111) surface  
15 was also calculated for comparison. The C and O adsorption energies on different surfaces were  
16 calculated to further investigate the reaction mechanism as well as the nature of the active sites. A  
17 Bader charge analysis and the calculation of the electronic density of states were performed to  
18 understand the nature of adsorbates binding to the surface.

19  
20  
21  
22  
23  
24  
25  
26  
27  
28  
29  
30  
31  
32  
33  
34  
35  
36  
37  
38  
39  
40 From these results we surmise the unique conclusion that the active center for the Boudouard  
41 reaction can be attributed to Mo while Pt serves in a role of preferentially collecting carbon. Such  
42 an observation has, to the best of our knowledge, hereto now not been described in the significant  
43 body of existing work on the Pt/Mo<sub>2</sub>C system. While the service of this mechanism in a practical  
44 continuous flow reaction system may not be readily apparent, this result informs the fundamental  
45 mechanism of a common side reaction and provides an important vantage point for carbon and  
46 coke formation.  
47  
48  
49  
50  
51  
52  
53  
54  
55  
56  
57  
58  
59  
60

## Methods

**Experiment.** Material synthesis and TAP experiments were performed as reported in our previous work.<sup>10</sup> Briefly, the Pt/Mo<sub>2</sub>C samples prepared with 50 and 100 ALD cycles are denoted as 50 Pt/Mo<sub>2</sub>C and 100 Pt/Mo<sub>2</sub>C respectively. The material was *ex situ* pretreated by flowing a gas mixture of 15% CH<sub>4</sub> in H<sub>2</sub> at a flow rate of 150 mL/min and a temperature of 590 °C for 4 h to reduce the Mo<sub>2</sub>C surface that might be oxidized in air. Before starting the pulsing experiment, the catalyst was heated in the TAP reactor, under vacuum, from room temperature to 400 °C to desorb any surface species; the temperature programmed desorption (TPD) spectra is shown in the Supporting Information (SI). Minor CO<sub>2</sub> release was observed which can be attributed to the surface oxygen formed during the ambient transfer and the surface carbon either from uncoordinated C in Mo<sub>2</sub>C or CH<sub>4</sub> decomposition in the reduction process. The catalysts were initially exposed to a sequence of CO pulses until the CO uptake reached a plateau followed by a TPD experiment to investigate the reaction of adsorbed CO at higher temperatures. Next, starting from the *in situ* TPD pretreated surface, the experimental temperature was linearly increased at a much slower rate (1 °C/min) from room temperature to 300 °C while pulsing CO. The exit flow pulse responses of unreacted CO and the CO<sub>2</sub> produced on the Mo<sub>2</sub>C, 50 Pt/Mo<sub>2</sub>C and 100 Pt/Mo<sub>2</sub>C catalysts were recorded in the temperature-programmed pulsing experiments. The morphology of Pt/Mo<sub>2</sub>C samples after TAP experiments were measured by TEM on a JEM-2100P electron microscope operating at 200 kV (JEOL Ltd., Tokyo, Japan).

It is important to note that the CO<sub>2</sub> produced in the pulsing experiment is mostly through the disproportionation process and the contribution of CO oxidation by the surface oxygen from the ambient is not significant. The reason is that the CO<sub>2</sub> fraction yield from converted CO was always less than 50% during the whole temperature programmed pulsing experiment. The

1  
2  
3 production of 1 mol CO<sub>2</sub> via CO oxidation by the surface oxygen only requires 1 mole CO.  
4  
5 Additionally, only CO desorption was observed and no CO<sub>2</sub> desorption was detected below 300  
6  
7 °C in the temperature programmed desorption (TPD) experiment with CO preadsorption on pure  
8  
9 Mo<sub>2</sub>C and 50 Pt/Mo<sub>2</sub>C (SI, Figure S5). In comparison, significant CO<sub>2</sub> was produced under the  
10  
11 condition of continuous CO pulsing on pure Mo<sub>2</sub>C and 50 Pt/Mo<sub>2</sub>C below 300 °C. Thus, if the  
12  
13 CO<sub>2</sub> produced in the temperature programmed pulsing experiment was mostly through CO  
14  
15 oxidation, significant CO<sub>2</sub> production would have been observed in the TPD experiment with CO  
16  
17 preadsorption.  
18  
19  
20

21  
22 More evidence of the Boudouard reaction was found in our DRIFTS experiment<sup>10</sup> with CO  
23  
24 purging on the studied materials (SI, Figures S1 and S2). The DRIFTS spectra collected right after  
25  
26 purging CO indeed clearly showed the CO<sub>2</sub> peaks. Also, there was no air or oxygen detected in  
27  
28 the down-stream mass spectra, indicating that the CO<sub>2</sub> was produced via the Boudouard reaction,  
29  
30 not CO oxidation.  
31  
32

33 **Electronic Structure Calculations.** The periodic DFT calculations were performed with the  
34  
35 Perdew–Burke–Ernzerhof (PBE) exchange-correlation functional<sup>31</sup> and the plane-wave basis sets  
36  
37 first using the Vienna ab initio simulation package (VASP).<sup>32,33,34</sup> The projector-augmented wave  
38  
39 (PAW) method<sup>35,36</sup> was employed to describe the interaction between the atomic cores and the  
40  
41 electrons. The 5*p* semi-core electrons for Pt and the 4*s* and 4*p* semi-core electrons for Mo were  
42  
43 treated as valence electrons. For the plane-wave basis sets, a kinetic energy cutoff of 520 eV was  
44  
45 chosen for the reactions on Pt (111), β-Mo<sub>2</sub>C (100) surfaces, and Pt/Mo<sub>2</sub>C interface. Previous  
46  
47 studies<sup>37,38,39</sup> showed that GGA functionals such as PBE fail to properly describe the interaction  
48  
49 between CO and Pt (111) surface due to the lack of dispersion corrections using the GGA  
50  
51 functionals. We performed static calculations for the PBE relaxed structures using the Meta GGA  
52  
53  
54  
55  
56  
57  
58  
59  
60

1  
2  
3 M06L functional<sup>40</sup> and the same basis sets employed for the relaxations. The M06L functional  
4 includes dispersion effects in its parameterization and correctly describes the CO adsorption on Pt  
5 (111) surface.<sup>37</sup>  
6  
7

8  
9  
10 The bulk lattice constant for the face-center-cubic (FCC) bulk Pt was optimized with  
11 Monkhorst-Pack k-meshes of  $15 \times 15 \times 15$ . The lattice constant was calculated to be  $a = 3.975 \text{ \AA}$   
12 with PBE, agreeing well with literature.<sup>41</sup> The lattice parameter is also consistent with the  
13 experimental value of  $3.92 \text{ \AA}$ .<sup>42</sup> For the slab, a large surface model with low CO coverage was  
14 selected as the amount of the injected molecules was much smaller than the number of active sites  
15 on the surface under the TAP conditions. The Pt (111) surface was modeled by four layers using  
16 a  $4 \times 4$  super cell with a  $5 \times 5$  k-point grid. The top two layers were relaxed in the surface  
17 optimization as well as the adsorption reactions. The vacuum distance between two slabs was  $12$   
18  $\text{\AA}$ . The adsorbed molecules were added only on one side of the slab.  
19  
20  
21  
22  
23  
24  
25  
26  
27  
28  
29

30  
31 The hexagonal  $\beta\text{-Mo}_2\text{C}$  forms a disordered crystal lattice from X-ray diffraction  
32 experiment.<sup>43,44</sup> Mo atoms form a hexagonal close packed array and C atoms statistically occupy  
33 one half of the octahedral interstitial sites. The most stable Mo-C-Mo-C stacking pattern has an  
34 eclipsed configuration.<sup>45, 46, 47,48</sup> In the following sections, the  $\text{Mo}_2\text{C}$  (100) surface denotes the  
35 HCP  $\beta\text{-Mo}_2\text{C}$  (100) surface. We selected the model proposed by Wang et al.<sup>23</sup> and a unit cell of  $2$   
36  $\times 2 \times 1$  size of the primitive cell was optimized. The  $5 \times 5 \times 6$   $\Gamma$ -centered Monkhorst-Pack k-point  
37 grid was used. The lattice constants were optimized to be  $2a = 6.062 \text{ \AA}$ ,  $2b = 6.049 \text{ \AA}$ , and  $c = 4.706$   
38  $\text{\AA}$ , which are consistent with the experiment values of  $a = b = 3.011 \text{ \AA}$  and  $c = 4.771 \text{ \AA}$ .<sup>49</sup> Our  
39 calculated lattice parameters are in agreement with the model used by Shi<sup>48</sup> in which the carbons  
40 atoms are in a different orientation. The supercell for  $\text{Mo}_2\text{C}$  slab was  $2 \times 2$  of the optimized unit  
41 cell. There are two different Mo terminated and one C terminated  $\text{Mo}_2\text{C}$  (100) surfaces. We select  
42  
43  
44  
45  
46  
47  
48  
49  
50  
51  
52  
53  
54  
55  
56  
57  
58  
59  
60

1  
2  
3 the most stable Mo-terminated Mo<sub>2</sub>C (100) surface to study the Boudouard reaction. The slab  
4 contains four Mo<sub>2</sub>C layers and the top two Mo<sub>2</sub>C layers are relaxed for the geometry optimization.  
5  
6 The CO adsorption on the eight slab layers gives a physisorption energy with a difference of only  
7  
8 0.01 eV. Thus, accurate results can be obtained from the calculations on the slab with four Mo<sub>2</sub>C  
9  
10 layers. The vacuum distance was selected as 12 Å. Since the optimized Mo<sub>2</sub>C surfaces are  
11  
12 stoichiometric, we used the following equation (1) proposed by previous work<sup>23,47,48</sup> to calculate  
13  
14 the cleavage energies:  
15  
16  
17

$$\sigma = (E_{\text{slab}} - n E_{\text{bulk}})/2A \quad (1)$$

18  
19 where  $E_{\text{slab}}$  and  $E_{\text{bulk}}$  are the total energies of the slabs and the bulk;  $n$  is the number of Mo<sub>2</sub>C units  
20  
21 in the slab and  $A$  is the surface area.  
22  
23  
24  
25

26 Based on the most stable Mo-terminated Mo<sub>2</sub>C (100) surface, we built a slightly tilted one  
27 layer 2 × 3 Pt slab by the adsorption of 12 Pt atoms on the surface. The building of this model  
28 started from the deposition of 6 Pt atoms and the most favorable additions are the C sites with the  
29 formation of Pt-C bonds. The addition of another 6 Pt atoms forms a tilted one layer (2 × 3) which  
30 is structurally close to the Pt (111) with slightly shorter Pt-Pt bond distances. We used this model  
31 to study CO reactions at the interface. For the Pt/Mo<sub>2</sub>C interface surface calculations, the vacuum  
32 distance was also set to 12 Å. One should be aware that this interface model does not directly  
33 model either 50 Pt/Mo<sub>2</sub>C or 100 Pt/Mo<sub>2</sub>C material. The HRTEM images show the average Pt  
34 particle size on 50 Pt/Mo<sub>2</sub>C and 100 Pt/Mo<sub>2</sub>C ranges from 2.0 to 2.5 nm.<sup>10</sup> Due to the high  
35 computational cost, it is nearly impossible to model 2 nm Pt nanoparticles on Mo<sub>2</sub>C support with  
36 DFT. The Pt nanoparticles on 50 Pt/Mo<sub>2</sub>C have more interface character and less domain of the  
37 Pt(111) surface compared to 100 Pt/Mo<sub>2</sub>C.<sup>10</sup>  
38  
39  
40  
41  
42  
43  
44  
45  
46  
47  
48  
49  
50  
51  
52  
53  
54  
55  
56  
57  
58  
59  
60

1  
2  
3 Geometries were relaxed until the residual force on each atom was 0.02 eV/Å. The  
4  
5 calculations for the isolated gas phase molecules and atoms were carried out with a 8.0 Å × 8.0 Å  
6  
7 × 8.0 Å unit cell and one k-point for the Brillouin zone. The adsorption energy ( $E_{\text{ads}}$ ) was calculated  
8  
9  
10 by equation (2):

$$E_{\text{ads}} = E_{\text{adsorbate/slab}} - E_{\text{adsorbate}} - E_{\text{slab}} \quad (2)$$

14 where,  $E_{\text{adsorbate/slab}}$  and  $E_{\text{slab}}$  are the total electronic energies of the slab at 0 K with and without the  
15  
16 adsorbate and  $E_{\text{adsorbate}}$  is the total electronic energy of the adsorbate in the gas phase. The climbing  
17  
18 image nudged elastic band (cNEB) method was used to locate the transition state.<sup>50,51</sup> The  
19  
20 transition state was characterized by the presence of one and only one imaginary frequency. A  
21  
22 Bader charge analysis<sup>52,53</sup> was performed to determine the local charges of atoms in the system.  
23  
24 Adsorbate vibrational frequencies were calculated using finite differences with a step size of 0.015  
25  
26 Å. The corresponding vibrations were used to compute the zero-point energy (ZPE) corrections  
27  
28 and vibrational partition functions for all adsorbed species and transition states. The detailed  
29  
30 descriptions for the derivation of CO transient pressure, free energy and rate constant calculations  
31  
32 are shown in Supporting Information. The local density of states (LDOS), electron localization  
33  
34 function (ELF),<sup>54,55</sup> and partial charge density (PCD) were calculated using 3 × 4 × 1  $\Gamma$ -centered  
35  
36 k-points to investigate the nature of bonding. All calculations have been performed on Idaho  
37  
38 National Laboratory Falcon clusters with an SGI ICE-X distributed memory system.  
39  
40  
41  
42  
43

## 44 **Experimental Results**

46  
47 **TPD with CO Preadsorption** The results for the TPD spectra with CO preadsorption at room  
48  
49 temperature are shown in the Supporting Information (Figure S5). Surprisingly, the per pulse CO  
50  
51 conversion on the 100 Pt/Mo<sub>2</sub>C catalyst (Figure S5b) is about 60% even after dosing of 5000 nmols  
52  
53 indicating that the plateau region represents an adsorption/desorption equilibrium. The total CO  
54  
55  
56  
57

uptake on 100 Pt/Mo<sub>2</sub>C is approximately 600 nmol and about 1/3 monolayer of surface metal atoms (Pt and Mo, see Supporting Information for the calculation of surface metal atoms). The total CO uptake on Mo<sub>2</sub>C and 50 Pt/Mo<sub>2</sub>C are comparable and are only approximately one half of that on 100 Pt/Mo<sub>2</sub>C. A broad CO desorption peak spanning from 50 °C to 250 °C was observed on all three materials. The total amount of CO desorbed up to 300 °C from the bare Mo<sub>2</sub>C support is comparable to that from the 50 Pt/Mo<sub>2</sub>C catalyst but is about one half of that from the 100 Pt/Mo<sub>2</sub>C sample. From our previous DRIFTS results,<sup>10</sup> the desorbed CO below 250 °C on 50 Pt/Mo<sub>2</sub>C are from the Mo<sub>2</sub>C sites. In addition, the CO added to the catalysts is observed to desorb as CO<sub>2</sub> below 300 °C only for the 4Pt/Mo<sub>2</sub>C sample with a peak maximum near 250 °C. The production of CO<sub>2</sub> during the temperature ramp indicated the role of Boudouard chemistry but was limited by the capacity for CO retention.

**Temperature Programmed Pulsing** The temperature programmed experiments with the continuous pulsing of CO on the clean surfaces of Mo<sub>2</sub>C, 50 Pt/Mo<sub>2</sub>C and 100 Pt/Mo<sub>2</sub>C are shown in Figure 1. While this data was presented previously,<sup>10</sup> the Pt-assisted carbon mediation mechanism had not been considered. Here we provide a more detailed kinetic analysis. Throughout the experiment, significant CO<sub>2</sub> production was observed on the bare Mo<sub>2</sub>C support at low temperature (<100 °C) in a process that quickly dissipated. The Pt-modified catalysts also showed low-temperature CO<sub>2</sub> production, but the intensity was much lower.

The CO conversion and fractional CO<sub>2</sub> yield during CO pulsing over the three samples are calculated and plotted as a function of temperature (Figure 1a and 1b). The fractional CO<sub>2</sub> yield is defined as the fraction of the adsorbed CO molecules being transformed into CO<sub>2</sub>. A basic evaluation of this data indicates that while the conversion of CO is generally the same for these materials, the presence of Pt results in remarkably distinct production trends for CO<sub>2</sub>. For all

1  
2  
3 catalysts the per pulse CO conversion is very high (>40%) throughout the experiment, especially  
4  
5 for the pure Mo<sub>2</sub>C support and the 50 Pt/Mo<sub>2</sub>C catalyst at low temperatures (<50 °C).  
6

7  
8 On a pure Mo<sub>2</sub>C surface, a simultaneous decrease in CO conversion and CO<sub>2</sub> production  
9  
10 is observed at low temperatures (below 50 °C). CO conversion drops as sites are occupied. Surface  
11  
12 oxygen is then consumed, slowing the production of CO<sub>2</sub>. However, as the temperature increases,  
13  
14 the declining conversion of CO passes through a turning point near 50 °C. The temperature  
15  
16 dependence of both CO and CO<sub>2</sub> exhibit an apparent plateau and near 225 °C, CO conversion  
17  
18 begins to drop.  
19  
20

21  
22 For 50 Pt/Mo<sub>2</sub>C, the CO conversion trend is the same as that on Mo<sub>2</sub>C below 200 °C. This  
23  
24 suggests that the same Mo active sites are used for CO conversion and the small Pt domains do  
25  
26 not directly contribute to low-temperature CO conversion. The production of CO<sub>2</sub>, however, is  
27  
28 not observed below 200 °C, as it is for Mo<sub>2</sub>C, indicating that Pt participates in the accumulation  
29  
30 and storage of CO. At 250 °C, the CO conversion of Mo<sub>2</sub>C begins dropping, but the Pt samples  
31  
32 continue increasing with temperature. This indicates that the Pt catalyst may assist in maintaining  
33  
34 CO conversion sites on Mo<sub>2</sub>C through collecting carbon.  
35  
36

37  
38 Compared to the reactions on the pure Mo<sub>2</sub>C and 50 Pt/Mo<sub>2</sub>C surfaces, the total conversion  
39  
40 of CO is lower and the rate of deactivation is slower on the 100 Pt/Mo<sub>2</sub>C surface at the low  
41  
42 temperatures (< 100 °C). CO might adsorb reversibly on the Pt (111) sites (not present on 50  
43  
44 Pt/Mo<sub>2</sub>C)<sup>10,29</sup> in addition to the Mo sites. The reversible adsorption decreases the low-temperature  
45  
46 CO conversion. In the low-temperature region, however, CO<sub>2</sub> production is observed with the  
47  
48 exception of the 50 Pt sample, suggesting that the 100 Pt sample must have sites that  
49  
50 disproportionate CO at the lower temperatures. This process declines with temperature, similar to  
51  
52 the case of Mo<sub>2</sub>C. The transition point where CO conversion begins increasing occurs at the higher  
53  
54  
55  
56  
57

1  
2  
3 temperature (100 °C). Above 100 °C, CO conversion is essentially the same for all three materials.  
4  
5 However, CO<sub>2</sub> production for the 100 Pt sample demonstrates a dramatic acceleration. Its  
6  
7 acceleration is shifted to the lower temperatures, compared to that of 50 Pt/Mo<sub>2</sub>C.  
8  
9

10        Figures 1c through 1f show the mass balance of converted CO by three different materials.  
11  
12 The total converted CO molecules can undergo two different pathways. One pathway is to  
13  
14 produced CO<sub>2</sub> via the Boudouard process with the residue of one C atom per CO<sub>2</sub> molecule formed.  
15  
16 The other pathway is to remain on the surface in the form of either physisorbed or chemisorbed  
17  
18 CO. The mass balance equation of converted CO can be written as:  $N_{\text{converted}} = N_{\text{C}} + N_{\text{CO}_2} + N_{\text{CO}}$ ;  
19  
20 where  $N_{\text{converted}}$  is the total conversion (adsorption + reaction),  $N_{\text{C}}$  is cumulative surface C atoms  
21  
22 from the Boudouard reaction,  $N_{\text{CO}_2}$  is the total CO<sub>2</sub> molecules produced, and  $N_{\text{CO}}$  is cumulative  
23  
24 surface CO. Here  $N_{\text{C}}$  is the same as  $N_{\text{CO}_2}$ .  $N_{\text{converted}}$  equals the difference of the CO pulsed into the  
25  
26 reactor and the CO out of the reactor detected by the mass spectrometer. One should be aware that  
27  
28  $N_{\text{C}}$  does not include the C from the CO which undergo chemisorption only and do not proceed to  
29  
30 form CO<sub>2</sub>. The cumulative surface carbonaceous species ( $N_{\text{carb}}$ , figure 1d) is the summation of  $N_{\text{C}}$   
31  
32 and  $N_{\text{CO}}$ .  
33  
34  
35  
36  
37

38        Figure 1c gives the total conversion of CO on three different materials during the  
39  
40 temperature programmed pulsing experiment. The total conversion is comparable on Mo<sub>2</sub>C and  
41  
42 50 Pt/Mo<sub>2</sub>C materials, which is ~ 200 nmol less than that on 100 Pt/Mo<sub>2</sub>C. The cumulative surface  
43  
44 carbonaceous species (Figure 1d) shows that more carbonaceous species were observed on 50  
45  
46 Pt/Mo<sub>2</sub>C than on Mo<sub>2</sub>C. This also indicates 50 Pt/Mo<sub>2</sub>C is less reactive to produce CO<sub>2</sub> than Mo<sub>2</sub>C  
47  
48 under the reaction temperature less than 300 °C. Figure 1e and 1f show the surface CO and C  
49  
50 accumulation with respect to temperature. The cumulative surface CO follows the order of 100  
51  
52 Pt/Mo<sub>2</sub>C > 50 Pt/Mo<sub>2</sub>C > Mo<sub>2</sub>C. The cumulative surface C is similar for 100 Pt/Mo<sub>2</sub>C and Mo<sub>2</sub>C  
53  
54  
55  
56  
57  
58  
59  
60

1  
2  
3 at the temperature lower than 150 °C. At temperatures above 150 °C, significantly more surface C  
4 atoms are accumulated on 100 Pt/Mo<sub>2</sub>C than on Mo<sub>2</sub>C. The cumulative surface C is not sufficient  
5  
6 for 50 Pt/Mo<sub>2</sub>C until 200 °C. If all CO underwent the Boudouard reaction, then one would expect  
7  
8 a constant CO<sub>2</sub> fractional yield of 0.5 according to the Boudouard reaction stoichiometry. In all  
9  
10 cases, however, the fractional yield is lower, indicating an additional pathway for CO storage.  
11  
12

13  
14 **Structural Characterization** The catalysts were retrieved after the TAP experiments and  
15  
16 subjected to TEM characterization in order to investigate potential structural changes and  
17  
18 deposition of carbon species during the TAP experiments. The representative TEM results on the  
19  
20 100 Pt/Mo<sub>2</sub>C catalysts (Figure 2) show considerable carbon formation on the surface of the  
21  
22 catalysts with multi-wall nanosheets or onion-like structures. It is important to note that the Pt  
23  
24 nanoparticles are encapsulated by multi-layers of carbon species, most likely graphene sheets in  
25  
26 view of its comparable layer distance to that of carbon nanotubes.<sup>56,57</sup> EDX analysis (shown in SI)  
27  
28 of the catalyst in the same region clearly shows that some of the Pt nanoparticles migrate onto the  
29  
30 surface of carbon structures.  
31  
32  
33  
34

### 35 **Theoretical Results**

36  
37 To understand the nature of active sites as well as the role of the deposited Pt nanoparticles,  
38  
39 DFT was used to calculate the potential energy surfaces of the Boudouard reaction on the pure  
40  
41 Mo<sub>2</sub>C surface and the Pt/Mo<sub>2</sub>C interface. The CO, C, and O adsorption energies as well as the  
42  
43 bond distances on three different surfaces are summarized in Table 1 and Figure 6. The calculated  
44  
45 rate constants for key steps are shown in Table 2. The optimized  $\beta$ -Mo<sub>2</sub>C (100) surface structures  
46  
47 and the surface energies are shown in Figure 3. The optimized structures for Pt/Mo<sub>2</sub>C interface are  
48  
49 shown in Figure 4. The potential energy surfaces (PESs) for Boudouard reaction on Pt (111), Mo<sub>2</sub>C  
50  
51 (100), and Pt/Mo<sub>2</sub>C surfaces are shown in Figures 5 and the SI. The calculated free energy surfaces  
52  
53  
54  
55  
56  
57  
58  
59  
60

1  
2  
3 on Mo<sub>2</sub>C (100), and Pt/Mo<sub>2</sub>C surfaces are also shown in the SI. The results with the PBE functional  
4 as well as the less stable structures for CO reactions on three different surfaces are shown in SI.  
5  
6 Unless otherwise specified, we use the M06L results for the following discussion. The calculated  
7  
8 partial charge densities are shown in Figure 7 and the LDOS and ELF figures are shown in the SI.  
9

10  
11 **Mo<sub>2</sub>C Surfaces and Pt/Mo<sub>2</sub>C Interfaces** Figure 3 shows the two different relaxed Mo-terminated  
12 and a C-terminated Mo<sub>2</sub>C (100) surfaces and their surface energies. The Mo-terminated surfaces  
13 are more stable than the C-terminated surface with a difference in surface energies of 0.33 J/m<sup>2</sup>.  
14  
15 The most stable Mo<sub>2</sub>C (100) surface has a stepped configuration. There are two different types of  
16 surface Mo atoms, upper-layer and lower-layer Mo's. The lower-layer Mo atoms are bonded to  
17 three C atoms with two C atoms in the first layer and one C atom in the second carbon layer. In  
18 contrast, the upper-layer Mo atoms are bonded with two C atoms in the first carbon layer. There  
19 are, in total, four different adsorption sites on this stepped surface: upper top (UT), upper bridge  
20 (UB), lower top (LT), and lower bridge (LB). The second lowest energy Mo-terminated Mo<sub>2</sub>C  
21 (100) surface is also a stepped surface. Both the upper-layer and lower-layer Mo atoms are bonded  
22 with two C atoms in the first carbon layer. The C-terminated surface has the highest cleavage  
23 energy, 0.96 J/m<sup>2</sup> higher than the most stable surface. The surface energies with the PBE functional  
24 are predicted to be ~ 0.8 J/m<sup>2</sup> less than the M06L results. Our calculated cleavage energies with  
25 PBE are slightly larger than previous work by ~ 0.4 J/m<sup>2</sup>, where a 400 eV cutoff energy was used.  
26  
27  
28  
29  
30  
31  
32  
33  
34  
35  
36  
37  
38  
39  
40  
41  
42  
43  
44  
45 23

46  
47 Figure 4 shows the Pt/Mo<sub>2</sub>C interface structures. The deposition of 6 Pt atom on the most  
48 stable Mo-terminated Mo<sub>2</sub>C (100) surface (6Pt@Mo<sub>2</sub>C) gives the structure shown in Figure 4a.  
49 The 6 Pt atoms are separated into two rows in a linear array with each Pt bonded to one C and four  
50 adjacent Mo atoms. The Pt-C bond distances range from 2.10 Å to 2.12 Å. The Pt-Mo bond  
51 distances are predicted to be 2.65 to 2.68 Å for the upper Mo's and 2.83 to 2.88 Å for the lower  
52  
53  
54  
55  
56  
57  
58  
59  
60

1  
2  
3 Mo's. The higher energy structures with 3 out of the 6 Pt atoms adsorbed on the upper bridge (UB)  
4 sites are shown in Supporting Information (SI). We calculated Pt adsorption energies with equation  
5  
6 (2) using the adsorbate of 6 Pt atoms. For the structures with three of 6 Pt atoms bonded to three  
7  
8 upper-layer Mo atoms and three Pt atoms, the Pt adsorptions energies are 1.89 and 3.01eV less  
9  
10 negative than the most stable one (Figure 4a) with the M06L functional. Starting from the most  
11  
12 stable 6Pt@Mo<sub>2</sub>C, the structure of a tilted one-layer Pt (2 × 3) on Mo<sub>2</sub>C (100) (12Pt@ Mo<sub>2</sub>C)  
13  
14 generated by the addition of an additional 6 Pt atoms is shown in Figure 4b. The Pt-Pt bond  
15  
16 distances range from 2.53 Å to 3.04 Å, which are comparable to the Pt-Pt bond distance of 2.82 Å  
17  
18 for the FCC Pt bulk in the current study and an experimental value of 2.76 Å<sup>58</sup> for the solid. For  
19  
20 the Pt (2 × 3) region on the interface, each of the Pt top, bridge, and hollow sites may be slightly  
21  
22 different as the one layer Pt (2 × 3) is not a perfect Pt (111) slab. Another 12Pt @ Mo<sub>2</sub>C structure  
23  
24 with the 9 Pt atoms more like one-layer Pt (3 × 3) (Figure 4c) is higher in energy by 1.39 eV.  
25  
26  
27  
28  
29

30 **CO Adsorption and Disproportionation** We first studied the Boudouard reaction on Pt (111)  
31  
32 (4×4) surface for the addition of two CO molecules and the coverage of 1/8 ML using the M06L  
33  
34 functional. The potential energy surfaces from both PBE and M06L functionals are shown in  
35  
36 Supporting Information. Consistent with the literature,<sup>37,39</sup> our M06L results show the top site is  
37  
38 preferred over the other sites, which is in agreement with experiment.<sup>59,60</sup> In contrast, PBE gives  
39  
40 the FCC site as the most stable adsorption site (Figure S13). The CO adsorption energy with PBE  
41  
42 on a 4×4 surface with a coverage of 1/16 ML (Table 1 and Figure S13) is slightly more exothermic  
43  
44 by up to 0.1 eV than previous reports with the CO coverage of 1/12 to ¼.<sup>37,38,39,61,62</sup> The  
45  
46 dissociation of CO on Pt (111) (4×4) surface is endothermic by 1.26 eV with M06L, which is in  
47  
48 reasonable agreement with the value of 0.9 eV,<sup>5</sup> which was calculated with the PW91 functional.  
49  
50  
51  
52  
53  
54 <sup>63,64</sup> The barrier energy for the dissociation of CO is calculated to be 4.25 eV from the CO  
55  
56  
57  
58  
59  
60

1  
2  
3 adsorbed structure. The addition of a second CO on the C and O preadsorbed surface still prefers  
4 a top site with the adsorption energy slightly lower by 0.6 eV compared to that on a clean surface.  
5  
6  
7 The formation of CO<sub>2</sub> occurs by surface O diffusion to the second CO with an energy barrier of  
8 0.73 eV at the M06L level. Although the overall Boudouard reaction process on Pt (111) is  
9 exothermic by -1.43 eV, the dissociation step to produce the 'reactive' surface O is a 1.26 eV  
10 endothermic step with a substantially high barrier energy of 4.25 eV. Thus, the Boudouard reaction  
11 will not occur readily on Pt (111) surface.  
12  
13  
14  
15  
16  
17  
18

19 *CO on  $\beta$ -Mo<sub>2</sub>C (100)* Figure 5 shows the potential energy surface for the Boudouard reaction on  
20 the most stable Mo-terminated Mo<sub>2</sub>C surface with M06L. The PBE results as well as the potential  
21 energy surfaces with higher energy intermediates are shown in the SI. CO adsorption on the  
22 stepped Mo<sub>2</sub>C (100) surface prefers a tilted configuration on an upper top (UT) Mo site. The  
23 adsorption energy is predicted to -2.19 eV and -2.15 eV with the M06L and PBE functionals  
24 respectively, and both functionals give the same site preference. Although, PBE fails to predict the  
25 correct adsorption site for the adsorption of CO on Pt (111) surface, it does describe the interaction  
26 between CO and Mo<sub>2</sub>C successfully. The CO adsorption energies on the upper bridge (UB) and  
27 the lower top (LT) sites are 0.36 and 1.37 less negative than the UT site. The tilted configuration  
28 for CO adsorption on Mo<sub>2</sub>C (100) surface is consistent with that on the HCP  $\beta$ -Mo<sub>2</sub>C (001) surface,  
29 <sup>65</sup> where the adsorption energy is predicted to be -2.61 eV with the PBE functional. Our calculated  
30 CO adsorption energy on  $\beta$ -Mo<sub>2</sub>C (100) surface is slightly more negative than that on  
31 orthorhombic Mo<sub>2</sub>C (001) surface which is predicted to be -1.85 eV with RPBE.<sup>66,67</sup>  
32  
33  
34  
35  
36  
37  
38  
39  
40  
41  
42  
43  
44  
45  
46  
47  
48

49 Different from CO dissociation on Pt (111), CO dissociation on Mo<sub>2</sub>C (100) is an  
50 exothermic process by -4.36 eV calculated using independent Mo<sub>2</sub>C (100)-C and Mo<sub>2</sub>C (100)-O  
51 calculations. The exothermicity for C and O co-adsorption on Mo<sub>2</sub>C (100) surface is -4.05 eV. The  
52  
53  
54  
55  
56  
57  
58  
59  
60

1  
2  
3 independent C and O adsorption calculations are performed to eliminate the role of the coverage  
4 effect of the adsorbate. Thus, the low coverage of adsorbed CO is favorable for the dissociation.  
5  
6 The most favorable site for C is the Mo LB site with C bonded to two lower Mo atoms and one C  
7 atom. The C adsorption energy is predicted to be -10.23 eV with M06L, which is more exothermic  
8 than C on the FCC site of Pt (111). Interestingly, the most favorable site for O adsorption is the  
9 Mo UB site and an O atom is bonded to two upper Mo atoms. The O adsorption energy is only 0.3  
10 eV less negative than that for C. Again, O adsorption on Mo<sub>2</sub>C (100) is also more exothermic than  
11 Pt (111). PBE gives a comparable CO dissociation energy with a difference of less than 0.2 eV  
12 from the M06L result. The dissociation energy on the Mo<sub>2</sub>C (100) surface is slightly more  
13 exothermic than that on the flat  $\beta$ -Mo<sub>2</sub>C (001) surface, which is predicted to -3.40 eV<sup>68</sup> with PBE.  
14  
15 The energy barrier for CO dissociation is predicted to be only 0.81 eV and the energy of the  
16 transition state structure is still below the reactant asymptotic energy of gas phase CO and pure  
17 Mo<sub>2</sub>C (100) slab. Thus, under low coverage conditions, CO should readily dissociate on clean  $\beta$ -  
18 Mo<sub>2</sub>C (100) surface to produce surface O atoms for further oxidation reactions.

19  
20  
21 The second CO addition also prefers an adjacent Mo UT site with a physisorption energy  
22 of -2.18 eV on the C and O preadsorbed Mo<sub>2</sub>C (100) surface, which is essentially the same as CO  
23 physisorption on the clean surface. CO<sub>2</sub> is produced from the surface O generated from the first  
24 CO and an adjacent CO with an energy barrier of 1.79 eV. CO<sub>2</sub> binding on Mo<sub>2</sub>C (100) surface  
25 forms a bidentate carbonate-type configuration with two O atoms bonded to two adjacent UT Mo  
26 atoms respectively. The CO<sub>2</sub> is now bent with  $\angle$  O-C-O = 134.3°. The respective Mo-O bond  
27 lengths are 1.955 Å and 2.194 Å. The energy required for CO<sub>2</sub> desorption is predicted to be 2.22  
28 eV. Similar CO<sub>2</sub> bending is also predicted on Mo-terminated  $\beta$ - Mo<sub>2</sub>C (001) surface and  $\angle$  O-C-O  
29 = 133°.<sup>7</sup> The corresponding CO<sub>2</sub> binding energy is predicted to be -1.38 eV with PBE, less  
30  
31  
32  
33  
34  
35  
36  
37  
38  
39  
40  
41  
42  
43  
44  
45  
46  
47  
48  
49  
50  
51  
52  
53  
54  
55  
56  
57  
58  
59  
60

1  
2  
3 exothermic than our result of -2.22 eV on Mo<sub>2</sub>C (100) surface. We also examined linear O=C=O  
4  
5 physisorption on the surface. The adsorption site is still the upper top with a tilted configuration  
6  
7 (SI). This tilted binding interaction is calculated to be only -0.46 eV, consistent with a physisorption  
8  
9 process.  
10

11  
12 *CO on Pt/Mo<sub>2</sub>C Interface* Figure 5 shows the potential energy surface for Boudouard reaction at  
13  
14 the Pt/Mo<sub>2</sub>C interface. CO dissociation starts from the adsorption on the Pt of the interface  
15  
16 followed by the diffusion of CO from the Pt to the Mo sites at the interface. The most favorable  
17  
18 CO adsorption takes place at the top site of the Pt atoms. This physisorption energy is predicted to  
19  
20 be -2.44 eV, which is more exothermic than those on the pure Pt (111) and Mo<sub>2</sub>C (100) surfaces.  
21  
22 which shows a significant synergistic effect between the deposited Pt and the Mo on a pure  $\beta$ -  
23  
24 Mo<sub>2</sub>C (100) surface. The bimetallic synergistic effect significantly changing the CO binding  
25  
26 energy on Pt nanoparticles is also reported on Pt shell on TiWC and TiWN core nanoparticles,  
27  
28 where the TiWC and TiWN cores weaken the strength of CO binding.<sup>69</sup> The dissociation of CO  
29  
30 leading to the formation of a surface O atom and a surface C atom on the deposited Pt atoms,  
31  
32 however, is endothermic by 1.06 eV.  
33  
34  
35  
36  
37

38 Thus, CO dissociation on the interface, if it occurs, is likely to take place at different sites,  
39  
40 potentially on the Mo sites via a preliminary step of CO diffusion from Pt to Mo sites. The CO  
41  
42 diffusion barrier from the Pt site to the Mo site is predicted to be 0.88 eV and most of this is due  
43  
44 to the endothermicity of the process. CO physisorption on the Mo top site is predicted to be  
45  
46 exothermic by -1.69 eV, which is less exothermic than that on the pure  $\beta$ -Mo<sub>2</sub>C (100) surface. It  
47  
48 is also less exothermic than the CO adsorption on the top site of Pt on the Pt/Mo<sub>2</sub>C interface by  
49  
50 0.75 eV. The molecular axis of CO is perpendicular to the Mo<sub>2</sub>C (100) surface, which is different  
51  
52 from the tilted configuration on the pure Mo<sub>2</sub>C (100) surface. The vertical configuration is mostly  
53  
54  
55  
56  
57

1  
2  
3 due to the conformation change of Mo<sub>2</sub>C (100) surface after the deposition of Pt atoms. In  
4 comparison to the endothermic process on the Pt of the Pt/Mo<sub>2</sub>C interface, the CO dissociation  
5 step on the Mo sites of the interface is still exothermic by -1.24 eV. The coadsorption of C and O  
6 on the interface has a three-coordinate configuration with two upper Mo atoms and one adjacent  
7 Pt atom for both C and O leading to a dissociation energy of -0.67 eV. Consistent with CO  
8 dissociation on the pure Mo<sub>2</sub>C (100) surface, a lower coverage of CO leads to a more negative  
9 dissociation energy. Again, on the Mo site of the interface, the CO dissociation is less exothermic  
10 than the pure Mo<sub>2</sub>C (100) surface, with a dissociation energy of -4.05 eV. The dissociation barrier  
11 from the adsorbed species is calculated to be 2.27 eV, which is larger than that on pure  $\beta$ -Mo<sub>2</sub>C  
12 (100) surface. This suggests that the CO dissociation at Pt/Mo<sub>2</sub>C interface takes place at a higher  
13 temperature than pure Mo<sub>2</sub>C (100) surface.  
14  
15  
16  
17  
18  
19  
20  
21  
22  
23  
24  
25  
26  
27

28 The addition of a second CO on an adjacent Mo top site is slightly different from the first  
29 CO addition. CO prefers a Mo-Pt bridge site with the C-Pt and C-Mo bond distances of 2.093 Å  
30 and 2.156 Å respectively. The  $\angle$  Mo-C-O bond angle distorts to 151.1°. The energy for CO  
31 physisorption is predicted to be -1.75 eV. The C-Mo bond distance is longer than that on the pure  
32 Mo<sub>2</sub>C (100) surface, consistent with a smaller adsorption energy on the interface than the pure  
33 (100) surface. Similar to the Pt (111) and pure Mo<sub>2</sub>C (100) surface, CO<sub>2</sub> is also produced from  
34 the surface O from the first CO dissociation and the second CO. The energy barrier is predicted to  
35 be 0.63 eV. CO<sub>2</sub> is chemisorbed at the interface with a tridentate configuration, which is similar  
36 to that on the pure  $\beta$ -Mo<sub>2</sub>C (100) surface with a difference of the C in CO<sub>2</sub> binding to an adjacent  
37 Pt with the bond distance of 1.986 Å. The Mo-O bond distances are comparable to that on the  
38 Mo<sub>2</sub>C (100) surface. The C-O bond lengths in CO<sub>2</sub> are elongated by 0.18 Å in comparison to those  
39 on the pure Mo<sub>2</sub>C (100) surface. The  $\angle$  O-C-O in adsorbed CO<sub>2</sub> is further bent to 122.8° as  
40  
41  
42  
43  
44  
45  
46  
47  
48  
49  
50  
51  
52  
53  
54  
55  
56  
57  
58  
59  
60

1  
2  
3 compared to that of  $134.3^\circ$  on pure  $\text{Mo}_2\text{C}$  (100) surface. The release of  $\text{CO}_2$  from the interface  
4  
5 requires 0.88 eV, which is much less than the  $\text{CO}_2$  binding energy on  $\text{Mo}_2\text{C}$  (100) surface (2.22  
6  
7 eV). The overall process to produce  $\text{CO}_2$  from two CO molecules is still an exothermic reaction  
8  
9 on the interface. Again, it is less exothermic than that on the pure  $\text{Mo}_2\text{C}$  (100) surface.  
10  
11

12 After the release of  $\text{CO}_2$ , the surface C atom bonded to the bridge site of upper Mo atoms  
13  
14 is likely to diffuse to the Pt region on the interface as the structure with C adsorption on a Pt hollow  
15  
16 site is more stable than that with C adsorption on a bridge Mo site. The migration barrier is  
17  
18 calculated to be 0.90 eV.  
19  
20

21 **C and O Adsorption** The adsorption energies of C and O on  $\text{Mo}_2\text{C}$  (100) surface and Pt/ $\text{Mo}_2\text{C}$   
22  
23 interface are helpful in understanding the active sites for the formation of  $\text{CO}_2$  and the collection  
24  
25 of surface C atoms. The results with the M06L functional are shown in Figure 6. The adsorption  
26  
27 energies with PBE as well as the results on Pt (111) are shown in Supporting Information. On the  
28  
29 most stable Mo-terminated  $\text{Mo}_2\text{C}$  (100) surface, the most exothermic site for C adsorption is the  
30  
31 lower bridge site with the formation of a strong C-C bond. C adsorption on a lower top Mo site is  
32  
33 2.47 eV less exothermic and forms an additional C-Mo bond with an upper top Mo atom  
34  
35 simultaneously. On Pt/ $\text{Mo}_2\text{C}$ , we calculated C adsorption on both the Pt sites and the Mo sites at  
36  
37 the interface. C adsorption on a Pt hollow site has a stronger binding than that on a Mo bridge site  
38  
39 at the interface. The C adsorption energies on different sites follow the order of  $\text{C}^*-\text{Mo}_2\text{C} > \text{Pt}^*-\text{Pt}/\text{Mo}_2\text{C} > \text{Mo}^*-\text{Pt}/\text{Mo}_2\text{C} > \text{Mo}^*-\text{Mo}_2\text{C}$ . C adsorption on Pt (111) is slightly less exothermic than  
40  
41 on the Pt region at the interface (see SI). This is probably due to the contribution of a synergistic  
42  
43 effect between Pt and Mo as noted above. Although, the formation of a C-C bond is most favorable  
44  
45 for C adsorption, the most favorable sites at the interface are most likely occupied by the deposited  
46  
47 Pt atoms as Pt atoms prefer the formation of Pt-C bonds instead of Pt-Mo bonds. Thus, at the  
48  
49  
50  
51  
52  
53  
54  
55  
56  
57  
58  
59  
60

Pt/Mo<sub>2</sub>C interface, the accumulated C atoms from the Boudouard reaction produced on the Mo sites most likely diffuse to the Pt region or surface C area if the active sites are not occupied by Pt atoms. The preference of Pt sites over Mo sites for C adsorption on the interface is partly attributed to the bond dissociation energy (BDE) of Pt-C that is larger than the Mo-C bond in the diatomic molecules.<sup>70</sup> The BDEs of diatomic Pt-C and Mo-C bonds are  $5.99 \pm 0.07$  and  $5.00 \pm 0.17$  eV respectively; both are weaker than the C-C bond energy in diatomic C<sub>2</sub> ( $6.41 \pm 0.16$  eV).<sup>70</sup>

O adsorption on the Mo<sub>2</sub>C (100) surface and the Pt/Mo<sub>2</sub>C interface (Figure 6) is different from C adsorption. The Mo bridge site is preferred for O adsorption on both the Mo<sub>2</sub>C (100) surface and the Pt-Mo<sub>2</sub>C interface. The most exothermic adsorption site is the Mo upper bridge site with an adsorption energy of -7.89 eV. The adsorption energy of the same site at the interface is predicted to be 1.63 eV less exothermic. We also tried adsorption on a lower bridge site with the formation of a C-O bond, but the adsorption energy is less exothermic than on the Mo sites. For the structure with O adsorption on a lower bridge Mo site, the C-O bond distance is predicted to be 1.550 Å, which is longer than that of CO with the distance of 1.16 Å. Similarly, the Mo-O bond distance of 2.324 Å is also longer than the Mo-O bond distance of 1.955 Å with O bonded to an upper bridge site. The least exothermic adsorption site in Figure 6 is the Pt hollow site with an adsorption energy of only -6.87 eV. Thus, the O adsorption energies on different sites follow the order of Mo\*-Mo<sub>2</sub>C > Mo\*-Pt/Mo<sub>2</sub>C > C\*-Mo<sub>2</sub>C > Pt\*-Pt/Mo<sub>2</sub>C. The O adsorption energy on the FCC site of Pt (111) (see SI) is 3.50 eV less exothermic than that on the most favorable site on Mo<sub>2</sub>C (100). Again, the preference of Mo sites over Pt sites for O adsorption at the interface is partly due to the fact that the BDE of Mo-O bond is larger than Pt-O bond. The BDEs of diatomic Pt-O and Mo-O are  $4.34 \pm 0.12$  and 6.29 eV respectively.<sup>70</sup> Thus, the structure with the formation of a Mo-O bond at the interface is more stable than that with the formation of a Pt-O bond.

**Bader Charge Analysis** A Bader charge analysis provides insights into the nature of the binding of CO, CO<sub>2</sub>, C and O to the surfaces. The calculated local atomic charges via Bader charge analysis on various CO, CO<sub>2</sub>, C and O adsorption structures as well as their adsorption energies are shown in the Supporting Information. The net charge is calculated from the difference of the electrons of a neutral atom and the calculated electrons of that atom in the system. For the adsorption of an atom, the net charge is also the adsorbate-surface charge transfer. For CO adsorption on Pt (111), Mo<sub>2</sub>C (100) and Pt/Mo<sub>2</sub>C surfaces, the adsorbate-surface charge transfer ranges from 0.02 e to 0.59 e with PBE. The charge transfer with M06L is similar to that with PBE. The charge transfer from Mo\* to CO is generally larger than that from Pt\* to CO and there is a reciprocal electron donation between CO and the active metal on the surface. The charge transfer does not correlate with the CO adsorption energies. The CO binding is a combination of  $\pi$ -backbonding (M to C) and  $\sigma$  donation (C to M). For CO adsorption on the Mo-Pt bridge site of Pt/Mo<sub>2</sub>C, the Mo donates electrons to CO and the Pt gains electrons from the C of CO. For CO<sub>2</sub> chemisorption on Mo<sub>2</sub>C (100), there is 0.96 e charge transfer from two upper Mo atoms to CO<sub>2</sub>. Similar charge transfer is predicted for a tridentate configuration for CO<sub>2</sub> chemisorption on Pt/Mo<sub>2</sub>C. Thus, the adsorbed CO<sub>2</sub> on Mo<sub>2</sub>C (100) and Pt/Mo<sub>2</sub>C surfaces behaves as CO<sub>2</sub><sup>-</sup>. The predicted O-C-O bond angles of 134° on Mo<sub>2</sub>C (100) surface is consistent with that in the gas phase anionic CO<sub>2</sub><sup>-</sup><sup>71</sup> and anionic CO<sub>2</sub> clusters with explicit H<sub>2</sub>O molecules,<sup>72</sup> which are predicted to be 135° and 137° respectively at the CCSD(T)<sup>73,74</sup> and MP2<sup>75,76</sup> levels. The interaction between CO<sub>2</sub> and Pt (111) is dominated by the van der Waals force as the charge transfer is insignificant.

The charge transfer for C and O adsorptions on various surfaces are also shown in the SI. Similar to the charge transfer from the surface to CO, more charge transfer to a C atom is predicted on Mo\* sites than that on Pt\* sites. Again, there is no significant correlation between C adsorption

1  
2  
3 energies and the corresponding charge transfers. The transition metal carbide M-C bond on a  
4 surface is characterized as a mixture of metallic, covalent and ionic bonds.<sup>77</sup> Thus, the adsorption  
5 energy is not only dependent on the charge transfer, but also the bonding nature itself mostly  
6 determined by different valence *d* electrons in the metal. For O adsorption, there is more electron  
7 transfer than for C adsorption, consistent with the higher electronegativity of O. There is a good  
8 correlation between the O adsorption energy on the active metal site and the charge transfer (Figure  
9 6). Thus, the M-O bond can be characterized as an ionic bond and the more charge transfer, the  
10 greater the adsorption energy is predicted. The larger adsorption energy on a Mo\* site than a Pt\*  
11 site is also consistent with the stronger BDE of a Mo-O than a Pt-O bond.

12  
13  
14  
15  
16  
17  
18  
19  
20  
21  
22  
23  
24 **Electronic Density of States** The LDOS is shown in the SI and mapped onto the structures as  
25 PCD in Figure 7. A different method of mapping the electrons to the structure, the ELF, is shown  
26 also shown in SI. While the PCD can be used to view a specific energy region of the LDOS, the  
27 ELF depicts all calculated electrons. In general, the LDOS shows the C adsorbate bond to the  
28 surface as a combination of ionic and covalent bonding and the chemical bond of O adsorbate to  
29 the surface is mostly ionic, consistent with the Bader charge analysis. Several regions exhibit  
30 covalent bonding as shown by the overlap in states, especially for C.

31  
32  
33  
34  
35  
36  
37  
38  
39  
40 The ELF diagrams in Figure S23 (a-d) shows that the adsorbed C prefers to bond  
41 covalently, recalling that moving from left to right in Figure 7 showed less stable structures. In  
42 Figure S23 (a), the adsorbed C is able to form a strong covalent bond with the surface C, indicated  
43 by a blue region showing a large concentration of charge surrounding two C atoms. In Figure S23  
44 (b), the C adsorbate also bonds covalently to Pt, although the ionic nature of the bonding is still  
45 observed as the most charge (shown in blue) is localized on C whereas less charge (shown in green)  
46 is localized on Pt. In Figure S23 (c), the adsorbate C is largely ionically bonded to the surface Mo  
47  
48  
49  
50  
51  
52  
53  
54  
55  
56  
57  
58  
59  
60

1  
2  
3 atoms which have almost no charge (shown in red). This structure (Figure S23 (c)) is only close  
4  
5 in adsorption energy to the previous structure (Figure S23 (b)) because the adsorbed C is still able  
6  
7 to bond covalently with Pt (in the (010) plane, perpendicular to the (100) plane shown in Figure  
8  
9 S23 (b)). The last C adsorption ELF (Figure S23 (d)) shows ionic bonding between the adsorbed  
10  
11 C and surface Mo.  
12  
13

14  
15         Narrowing the energy window to -2 eV relative to the Fermi energy in Figure 7 (a-d) shows  
16  
17 that the electron densities most likely to be involved in continuing the reacting are localized on the  
18  
19 C-adsorption structures. There is a general trend of structures with less charge on the adsorbed C  
20  
21 in this energy region being more stable. While the C in Figure 7 (a) is shown to still be active, it is  
22  
23 likely the most stable structure as shown by the strong covalent bonding in the ELF. The most  
24  
25 stable C adsorption on the Pt-Mo<sub>2</sub>C (Figure 7 (b)) shows that the C has very little charge (shown  
26  
27 in yellow). The adsorbed C in Figure 7 (c) shows the covalent nature of the M-C bond as the C  
28  
29 orbitals deform slightly towards the surface Mo. This C contains more active electrons than in  
30  
31 Figure 7 (b), exhibited by a green region. In the last C adsorption PCD (Figure 7 (d)), the C remains  
32  
33 highly active, shown by regions of blue.  
34  
35  
36

37  
38         Figure 7 (e-h) shows that the O prefers to have the most charge, without sharing electrons  
39  
40 with the surrounding atoms. Thus, the M-O bond has more ionic character than the M-C bond. An  
41  
42 energy window of -8 to -5 eV was selected to investigate the O adsorbate structures as this region  
43  
44 shows the most variation in the LDOS (Figure S22 e-h). Figure 7 (e) shows ionic bonding with  
45  
46 charge localized on O and some covalent character as the charge density deforms towards the  
47  
48 surface Mo atoms. Moving from Figure 7 (f) through Figure 7 (h) shows the deformation towards  
49  
50 the metal reduced until the charge is localized completely on the O adsorbate.  
51  
52  
53  
54  
55  
56  
57

**Calculated Rate Constants** On the basis of the above results, the essential reaction steps can be summarized in the following reaction sequence, where \* represents an active site on the Mo<sub>2</sub>C catalyst:

1.  $2(\text{CO}(\text{g}) + * \rightarrow \text{CO}^*)$  Adsorption (Physisorption)
2.  $\text{CO}^* + * \rightarrow \text{C}^* + \text{O}^*$  Disproportionation (and deactivation of 1 metal site)
3.  $\text{CO}^* + \text{O}^* \rightarrow 2* + \text{CO}_2(\text{g})$  CO<sub>2</sub> formation
4.  $\text{C}^* + *_{\text{Pt}} \rightarrow * + \text{C}^*_{\text{Pt}}$  Carbon collection on Pt and regeneration of metal site

Steps (1, 2 and 3) can proceed solely on the Mo<sub>2</sub>C material. This pathway leads to the deactivation of 1 metal site with the deposition of a carbon atom. The addition of Pt in step 4 enables a complete catalytic cycle with the regeneration of the active disproportionation site by collection of the C species.

Transition state theory<sup>78</sup> was employed to estimate the rate constants based on the calculated electronic energies. The various terms used the harmonic vibrational frequencies and the rigid rotor approximation. The calculated rate constants for the key steps on  $\beta$ -Mo<sub>2</sub>C (100), Pt/Mo<sub>2</sub>C, and Pt (111) surfaces with both PBE and M06L functionals are shown in Table 2. One should be aware that the rate constant for the reaction with gas phase CO involved varies along the curve of the transient pressure with respect to the time in each pulse. In addition, our experimental conditions are far from equilibrium (backward reactions can be neglected). The transient behavior of the gas pressure on the catalyst surface at selected temperature of 25, 100, 200, 300 °C is shown in the Supporting Information (Figure S3). We chose one half of the maximum pressure for each temperature as a representative pressure to investigate the different reaction rate on different materials. We used the effective activation energy for the reactions

1  
2  
3 involving the gas phase CO. The calculated rate constants with PBE and M06L are comparable for  
4  
5 the studied reactions.  
6

7  
8 On the  $\beta$ -Mo<sub>2</sub>C (100) surface, the rate constants for the dissociation of CO are sufficiently  
9  
10 high at the experimental temperatures to generate surface O species for the further CO<sub>2</sub> formation.  
11  
12 With large rate constants, the dissociation of CO is mostly a diffusion-controlled step rather than  
13  
14 an activation-controlled step on the  $\beta$ -Mo<sub>2</sub>C (100) surface. The formation of CO<sub>2</sub> is predicted to  
15  
16 be a slower step compared to the dissociation of CO. On Pt/Mo<sub>2</sub>C, the rate limiting step is the  
17  
18 dissociation of CO and the formation of CO<sub>2</sub> is a much faster step than the dissociation. CO  
19  
20 dissociation on Pt/Mo<sub>2</sub>C is much slower than that on Mo<sub>2</sub>C based on the calculated rate constants.  
21  
22 The diffusion rate constants for both CO diffusion from \*<sub>Pt</sub> to \*<sub>Mo</sub> and C diffusion from \*<sub>Mo</sub> to \*<sub>Pt</sub>  
23  
24 are large at temperatures above 200 °C. The results for Pt (111) are very different. The rate  
25  
26 constants for the CO dissociation on Pt (111) are so small that this process is unlikely to occur  
27  
28 under experimental temperatures lower than 300 °C. In comparison, the CO<sub>2</sub> formation step is a  
29  
30 much faster step on Pt (111), and is also faster than that on both  $\beta$ -Mo<sub>2</sub>C (100) and Pt/Mo<sub>2</sub>C. The  
31  
32 calculated rate constants indicate that the Boudouard reaction is unlikely to occur on the Pt domain  
33  
34 under the current experimental conditions. The Boudouard reaction on  $\beta$ -Mo<sub>2</sub>C (100) is fast but is  
35  
36 limited by the deactivation of residual C atoms.  
37  
38  
39  
40  
41

42 **Discussion** On pure Mo<sub>2</sub>C, significant CO<sub>2</sub> is produced at temperatures below 50 °C, which  
43  
44 is consistent with our calculations with a substantial exothermicity for the Boudouard reaction.  
45  
46 The energy barrier for the chemisorption of CO is also below the reactant asymptote, which  
47  
48 indicates that CO readily dissociates on a pure Mo<sub>2</sub>C surface. The fact that CO conversion as well  
49  
50 as CO<sub>2</sub> production drop quickly can be attributed to the active lower-level Mo sites on the pure  
51  
52 Mo<sub>2</sub>C surface that are occupied quickly by the residual C atoms from the Boudouard reaction. This  
53  
54  
55  
56  
57

1  
2  
3 surface deactivation process is expected to take place rapidly with the low energy barrier of the  
4  
5  
6 disproportionation process.

7  
8 The amount of CO conversion observed on 50 Pt/Mo<sub>2</sub>C is nearly identical to that on pure  
9  
10 Mo<sub>2</sub>C at temperatures below 200 °C; this indicates that a small amount of Pt does not change the  
11  
12 storage capacity of CO on Mo<sub>2</sub>C. However, the deposition of a small amount of Pt on Mo<sub>2</sub>C  
13  
14 significantly decreases the production of CO<sub>2</sub> (Figure 1b) at temperatures below 200 °C. To some  
15  
16 extent, the deposited Pt nanoclusters block the active lower-layer Mo sites for the dissociation of  
17  
18 CO as the deposited Pt atoms prefer the more stable lower bridge sites with the formation of Pt-C  
19  
20 bonds (Figure S22). Significant production of CO<sub>2</sub> on 50 Pt/Mo<sub>2</sub>C is not observed until the  
21  
22 experimental temperatures exceed 250 °C, which is due to a larger barrier for CO dissociation for  
23  
24 the Boudouard reaction predicted on Pt/Mo<sub>2</sub>C.  
25  
26  
27

28  
29 On 100 Pt/Mo<sub>2</sub>C, CO conversion shows a minor decline as temperature increases to 100  
30  
31 °C, which is consistent with our calculations that CO adsorption preferentially takes place on Pt  
32  
33 sites at the Pt/Mo<sub>2</sub>C interface in our 12Pt@Mo<sub>2</sub>C model and that the production of a small amount  
34  
35 of CO<sub>2</sub> does not deactivate the active sites significantly. It is important to note that the active sites  
36  
37 on Pt nanoparticles per unit area are larger than pure Mo<sub>2</sub>C as all surface Pt atoms are active for  
38  
39 CO adsorption. The production of CO<sub>2</sub> on 100 Pt/Mo<sub>2</sub>C is greater than that on 50 Pt/Mo<sub>2</sub>C at  
40  
41 temperatures below 300 °C because the 50 Pt/Mo<sub>2</sub>C has more limited CO storage capacity; this  
42  
43 limits the production of CO<sub>2</sub> as the formation of one mole of CO<sub>2</sub> requires two moles of CO. CO<sub>2</sub>  
44  
45 production is dependent on both the activation energy and the CO surface concentration. At  
46  
47 temperatures lower than 150 °C, the factor of activation outweighs the CO concentration and the  
48  
49 CO<sub>2</sub> yield on three materials follows the order of Mo<sub>2</sub>C > 100 Pt/Mo<sub>2</sub>C > 50 Pt/Mo<sub>2</sub>C. At  
50  
51  
52  
53  
54  
55  
56  
57  
58  
59  
60

1  
2  
3 temperatures between 150 °C and 300 °C, both factors contribute the CO<sub>2</sub> production, which  
4 follows a different order: 100 Pt/Mo<sub>2</sub>C > Mo<sub>2</sub>C > 50 Pt/Mo<sub>2</sub>C.  
5  
6

7  
8 The total conversion of CO (Figure 1c) on different materials follows the order of Mo<sub>2</sub>C <  
9 50 Pt/Mo<sub>2</sub>C < 100 Pt/Mo<sub>2</sub>C. The more Pt deposited, the greater the storage capacity for CO  
10 adsorption as surface C atoms of Mo<sub>2</sub>C are not active for CO adsorption and the surface Pt atoms  
11 as well as the Pt-Mo interface are active for CO storage. The estimate of the total number of surface  
12 metal atoms (SI) also shows more active sites for CO adsorption on 100 Pt/Mo<sub>2</sub>C than on 50  
13 Pt/Mo<sub>2</sub>C. CO readily dissociates on a β-Mo<sub>2</sub>C (100) surface at a low coverage from our DFT  
14 calculation, which suggests one dissociated CO occupies two active Mo sites. In addition, CO does  
15 not dissociate on Pt (111) surface under experimental conditions. Thus, the 100 Pt/Mo<sub>2</sub>C with  
16 greater Pt (111) domain has a larger capacity to store CO.  
17  
18  
19  
20  
21  
22  
23  
24  
25  
26  
27

28  
29 With respect to the accumulation of surface C atoms, a slightly smaller amount of C atoms  
30 are produced on 100 Pt/Mo<sub>2</sub>C compared to pure Mo<sub>2</sub>C below 150 °C as the larger energy barrier  
31 of CO disproportionation on Pt/Mo<sub>2</sub>C leading to the slower reaction rate for the production of CO<sub>2</sub>.  
32  
33 At temperatures greater than 175 °C, more CO<sub>2</sub> production results in greater accumulation of  
34 surface C on 100 Pt/Mo<sub>2</sub>C. Following the experiment, TEM observed C accumulation around Pt  
35 nanoparticles on 100 Pt/Mo<sub>2</sub>C is also consistent with the C adsorption energies on Pt sites being  
36 more exothermic than that of Mo. A similar phenomenon was reported in carbon nanotube  
37 synthesis by the decomposition of CH<sub>4</sub> on Mo/Co/MgO catalysts at temperatures higher than 650  
38 °C.<sup>79</sup> The active Co sites on Co/MgO catalysts could be poisoned by carbon deposition due to the  
39 rate of CH<sub>4</sub> decomposition reaction larger than the rate of graphene formation. The addition of Mo  
40 component is able to slow down CH<sub>4</sub> decomposition step and avoids the deactivation of Co.  
41  
42  
43  
44  
45  
46  
47  
48  
49  
50  
51  
52  
53  
54  
55  
56  
57  
58  
59  
60

1  
2  
3 In our previous work, TPD DRIFT experiments<sup>10</sup> with CO preadsorption under flow  
4 conditions showed that higher temperatures are needed to desorb CO on 50 Pt/Mo<sub>2</sub>C than on 100  
5 Pt/Mo<sub>2</sub>C. This is consistent with the calculated CO adsorption energies on the Pt (111) surface and  
6 the Pt/Mo<sub>2</sub>C surface with the former having weaker binding than the latter. The CO binding energy  
7 is predicted to be -1.53 eV on the Pt (111) surface (SI) as compared to CO adsorption energies of  
8 -2.44 and -1.75 eV on the Pt and Pt-Mo sites at the Pt/Mo<sub>2</sub>C interface (Figure 5 and Table 1, the  
9 first and second CO adsorption respectively). From the characterization in our previous study<sup>10</sup>,  
10 the Pt nanoparticles on 100 Pt/Mo<sub>2</sub>C are expected to have greater Pt(111) domains which are  
11 weaker for binding CO. In comparison with thinner Pt nanoparticles that were more dispersed,<sup>10</sup>  
12 the 50 Pt/Mo<sub>2</sub>C sample may generate more bimetallic Mo-Pt interface for stronger CO adsorption  
13 and the desorption of CO thus requires higher temperature.  
14  
15  
16  
17  
18  
19  
20  
21  
22  
23  
24  
25  
26  
27

28 The DFT results describing C, O, CO and CO<sub>2</sub> species can also be helpful to understand  
29 the WGS performance on pure Mo<sub>2</sub>C nanotubes, 50 Pt/Mo<sub>2</sub>C and 100 Pt/Mo<sub>2</sub>C observed in our  
30 previous experiments under flow conditions.<sup>10</sup> Nagai and Tominaga<sup>80</sup> predicted that the WGS  
31 reaction on the β-Mo<sub>2</sub>C(001) slab begins with the dissociation of H<sub>2</sub>O into surface H and O atoms  
32 followed by CO oxidation by oxygen and surface recombination of H atoms leading to the  
33 formation of CO<sub>2</sub> and H<sub>2</sub> using DFT. The formation of CO<sub>2</sub> was calculated to be the rate  
34 determining step. In this work, CO readily dissociates on the Mo<sub>2</sub>C nanotube modeled with the β-  
35 Mo<sub>2</sub>C(100) surface and high temperatures are needed for the recombination of dissociated C and  
36 O atoms. However, the WGS is an exothermic reaction at 298 K with a free reaction energy of -  
37 0.29 eV;<sup>81</sup> also high temperature is favorable for the reverse water gas shift (RWGS) reaction. This  
38 helps to explain why experimentally we observed that pure Mo<sub>2</sub>C nanotubes were not as efficient  
39 as Pt/Mo<sub>2</sub>C materials in regards to the WGS performance.<sup>10</sup> The flow experiment<sup>10</sup> also shows  
40  
41  
42  
43  
44  
45  
46  
47  
48  
49  
50  
51  
52  
53  
54  
55  
56  
57  
58  
59  
60

1  
2  
3 that a higher WGS reaction rate takes place on 50 Pt/Mo<sub>2</sub>C than on 100 Pt/Mo<sub>2</sub>C at temperatures  
4  
5 above 300 °C. Our calculations predict that the CO binding is stronger on 50 Pt/Mo<sub>2</sub>C than on 100  
6  
7 Pt/Mo<sub>2</sub>C, which suggests that the CO binding energies correlate with the WGS reaction rate on  
8  
9 50 Pt/Mo<sub>2</sub>C and 100 Pt/Mo<sub>2</sub>C materials. A stronger CO binding correlates with a higher reactivity  
10  
11 of WGS reaction on 50 Pt/Mo<sub>2</sub>C as compared to a weaker CO binding and a lower reactivity on  
12  
13 100 Pt/Mo<sub>2</sub>C. The correlation between the binding energy and the reactivity has been reported for  
14  
15 the hydrogenation of CO<sub>2</sub> on Pt, Pt/SiO<sub>2</sub> and Pt/TiO<sub>2</sub>,<sup>82</sup> where the material with stronger binding  
16  
17 of CO<sub>2</sub> shows more reactive for the reaction.  
18  
19  
20

21  
22         Orthorhombic Mo<sub>2</sub>C and Mo<sub>2</sub>C-supported copper clusters are reported to be active for the  
23  
24 CO<sub>2</sub> hydrogenation reactions.<sup>7,8</sup> It is interesting to note that CO<sub>2</sub> dissociation readily occurs with  
25  
26 the breaking of a C-O bond and formation of CO on an orthorhombic Mo<sub>2</sub>C (001) surface.<sup>7</sup> In  
27  
28 current work, CO<sub>2</sub> formation from the reaction of CO with surface O was observed. The process  
29  
30 of CO<sub>2</sub>\* → CO\* + O\* on an orthorhombic Mo<sub>2</sub>C (001) surface was reported to be exothermic by  
31  
32 ~ 3.0 eV with PBE. In comparison, the reaction energy of CO<sub>2</sub>\* + C\* + \* → CO\* + O\* + C\* on  
33  
34 the pure β-Mo<sub>2</sub>C (100) and Pt/Mo<sub>2</sub>C surfaces in this work is predicted to be only -0.86 eV and  
35  
36 0.07 eV respectively with PBE (SI). The different reaction energies are most likely due to different  
37  
38 CO<sub>2</sub> binding energies; CO<sub>2</sub> binding energies on pure β-Mo<sub>2</sub>C (100) and Pt/Mo<sub>2</sub>C surfaces are  
39  
40 predicted to be 2.43 eV and 0.84 eV, which are smaller than the binding energy of 3.27 eV on an  
41  
42 orthorhombic Mo<sub>2</sub>C (001) surface predicted with the PBE functional. Thus, the reactivity of CO<sub>2</sub>  
43  
44 on the Mo<sub>2</sub>C material is significantly affected by the CO<sub>2</sub> binding strength and varies significantly  
45  
46 on different surfaces.  
47  
48  
49  
50

51  
52         Similarly, CO and C adsorption on various Mo<sub>2</sub>C surfaces also behave differently. Wang  
53  
54 and Jiao studied CO adsorption and dissociation on a variety of orthorhombic Mo<sub>2</sub>C surfaces.<sup>22</sup>  
55  
56  
57  
58  
59  
60

1  
2  
3 Generally, they found that CO dissociation reaction on the surface with a stronger CO binding  
4 energy has a smaller reaction energy barrier. The dissociation is not always thermodynamically  
5 more favorable than adsorption. The different reactivities of different hexagonal  $\beta$ -Mo<sub>2</sub>C surfaces  
6  
7 have been predicted for the activation of H<sub>2</sub>, O<sub>2</sub>, H<sub>2</sub>O, CO<sub>2</sub>, CO, and small hydrocarbon molecules  
8  
9 and a  $\beta$ -Mo<sub>2</sub>C (001) surface is reported to be more reactive than a  $\beta$ -Mo<sub>2</sub>C (101) surface.<sup>26</sup> Also,  
10  
11 C adsorption is more exothermic on a more reactive  $\beta$ -Mo<sub>2</sub>C (001) surface than on a  $\beta$ -Mo<sub>2</sub>C (101)  
12  
13 surface which is predicted with PBE.  
14  
15  
16  
17  
18

19 The surface dependent reactivity is helpful to explain the phenomenon of Pt as carbon  
20 collector from our experimental results. Our CO dissociation on a  $\beta$ -Mo<sub>2</sub>C (100) surface with an  
21 exothermicity of -4.05 eV is more exothermic than that on a  $\beta$ -Mo<sub>2</sub>C (001) surfaces with a  
22 dissociation energy of -3.40 eV<sup>24</sup> as predicted with PBE. CO adsorption on  $\beta$ -Mo<sub>2</sub>C (001) is  
23 predicted to be more stable than that on  $\beta$ -Mo<sub>2</sub>C (101) with PBE.<sup>65</sup> Also, the cleavage energy  
24 predicted by PBE follows the order of  $\beta$ -Mo<sub>2</sub>C (100) >  $\beta$ -Mo<sub>2</sub>C (001) >  $\beta$ -Mo<sub>2</sub>C (101).<sup>23</sup> Thus, the  
25 stable  $\beta$ -Mo<sub>2</sub>C (100) surface selected in this work is most likely one of the very reactive surfaces  
26 on the Mo<sub>2</sub>C nanotube. The deposited Pt nanoparticles prefer the formation of Pt-C bonds and  
27 occupy the most reactive sites, C\*-Mo<sub>2</sub>C for C adsorptions on the pure Mo<sub>2</sub>C (100) surface. The  
28 residual carbon atoms from the Boudouard reaction on Pt/Mo<sub>2</sub>C most likely adsorb other different  
29 active sites. In current work, C adsorption on the C\*-Mo<sub>2</sub>C sites of other less active surfaces is  
30 most likely less exothermic than that on a  $\beta$ -Mo<sub>2</sub>C (100) surface and is also probably less  
31 exothermic than on the Pt sites of Pt/Mo<sub>2</sub>C material. Thus, the deposited Pt particles on Pt/Mo<sub>2</sub>C  
32 were able to absorb residual carbon atoms in the Boudouard process although the C adsorption  
33 energy on Pt\*-Pt/Mo<sub>2</sub>C is less exothermic than on C\*-Mo<sub>2</sub>C (100).  
34  
35  
36  
37  
38  
39  
40  
41  
42  
43  
44  
45  
46  
47  
48  
49  
50  
51  
52  
53  
54  
55  
56  
57  
58  
59  
60

1  
2  
3 The role of Pt nanoparticles as a carbon collector may be helpful for the design of new  
4 catalytical materials. Carbon and coke formation resulting in deactivation of catalysts is generally  
5 unavoidable in various industrial processes such as CO methanation<sup>83</sup> and steam reforming.<sup>84</sup> The  
6 Boudouard reaction is also an important side reaction in many catalytic processes.<sup>85</sup> For such  
7 processes, the doping of a small amount of Pt on the catalytic active species could be potentially  
8 useful to mitigate the deactivation if C atoms prefer to adsorb on the Pt domain rather than the  
9 catalytic active sites. Admittedly, practical implementation in a continuous process is not  
10 immediately apparent and the surprising feature of carbon collection mechanism may be more  
11 useful for fundamental understanding of the role of different active sites in multicomponent  
12 catalysts.  
13  
14  
15  
16  
17  
18  
19  
20  
21  
22  
23  
24  
25

## 26 **Conclusions**

27  
28 DFT studies on the potential energy surfaces of the Boudouard reaction on  $\beta$ -Mo<sub>2</sub>C (100),  
29 Pt(111) and Pt/Mo<sub>2</sub>C surfaces have been used to support the hypothesis of Pt-assisted carbon  
30 remediation of Mo<sub>2</sub>C active sites originally derived from transient kinetic experimental  
31 observations.<sup>10</sup> The model of 12Pt@Mo<sub>2</sub>C was used to simulate the reactions on the Pt  
32 nanoparticle-supported Mo<sub>2</sub>C nanotubes and the results are consistent with experiments. From  
33 temperature-programmed CO pulsing experiments using the TAP technique, the production of  
34 CO<sub>2</sub> on both pure Mo<sub>2</sub>C and Pt/Mo<sub>2</sub>C was observed to proceed via the Boudouard reaction. The  
35 Boudouard reaction begins with the dissociation of adsorbed CO on Mo sites to generate surface  
36 C and O species. The active O species then oxidize another adsorbed CO to form CO<sub>2</sub>. After the  
37 release of CO<sub>2</sub>, residual surface C atoms deactivate the Mo sites on pure Mo<sub>2</sub>C. In contrast, the  
38 addition of Pt nanoparticles to Mo<sub>2</sub>C enables collection of surface C atoms and help reactivate the  
39 Mo sites. C atom migration to the Pt region is favorable according to our DFT calculations. The  
40  
41  
42  
43  
44  
45  
46  
47  
48  
49  
50  
51  
52  
53  
54  
55  
56  
57  
58  
59  
60

1  
2  
3 deposited Pt nanoparticles also increase the storage capacity of CO, making 100 Pt/Mo<sub>2</sub>C, with  
4 greater Pt(111) domains, more productive to form CO<sub>2</sub> than 50 Pt/Mo<sub>2</sub>C. The maximum CO<sub>2</sub>  
5 production rate on 50 Pt/Mo<sub>2</sub>C takes place at a higher temperature than 100 Pt/Mo<sub>2</sub>C due to a  
6 stronger CO binding strength at the interface.  
7  
8  
9

10  
11  
12 Our calculated CO adsorption energies on Pt(111), pure Mo<sub>2</sub>C and the Pt/Mo<sub>2</sub>C interface  
13 help explain the different WGS performance among bare Mo<sub>2</sub>C nanotubes and those with uniquely  
14 sized Pt-domains.<sup>10</sup> The reactivities of 50 Pt/Mo<sub>2</sub>C and 100 Pt/Mo<sub>2</sub>C correlate with the CO  
15 adsorption energies; the catalyst with a strong CO binding is more reactive for the WGS reaction.  
16  
17 These CO adsorption energies may be useful references for understanding the selectivity of CO<sub>2</sub>  
18 hydrogenation and other reactions on Pt/Mo<sub>2</sub>C and related materials where CO is an intermediate.  
19  
20 The role of Pt acting as a carbon collector presents an alternative viewpoint of the mechanistic role  
21 of cooperative active centers that hereto now has not been expressed for the Pt/Mo<sub>2</sub>C system.  
22  
23  
24  
25  
26  
27  
28  
29

### 30 31 **ORCID**

32  
33 Zongtang Fang: 0000-0001-6034-1083

34  
35 Lucun Wang: 0000-0002-4930-8618

36  
37 Shuai Tan: 0000-0003-3200-7875

38  
39 Dongmei Li: 0000-0002-0529-9203

40  
41 David A. Dixon: 0000-0002-9492-0056

42  
43 Rebecca Fushimi: 0000-0002-7570-0234

### 44 45 46 47 **Notes**

48  
49 The authors declare no competing financial interest.

50  
51  
52 **Acknowledgement** ZF are thankful to Dr. Shenggang Li for fruitful discussions of the  
53 computational results. ZF, LW, DL, LL and RF acknowledge the support of the INL Laboratory  
54  
55

1  
2  
3 Directed Research & Development (LDRD) Program under DOE Idaho Operations Office contract  
4 no. DE-AC07-05ID14517. Additionally, transient kinetic tools developed through the support of  
5  
6 the U.S. Department of Energy, Office of Energy Efficiency and Renewable Energy (EERE),  
7  
8 Advanced Manufacturing Office Next Generation R&D Projects under contract no. DE-AC07-  
9  
10 05ID14517 were utilized. DAD was supported by the US Department of Energy, Office of Basic  
11  
12 Energy Sciences, Division of Chemical Sciences, Geosciences and Biosciences, Catalysis  
13  
14 Sciences under a subcontract from the Pacific Northwest National Laboratory. DAD thanks the  
15  
16 Robert Ramsay Chair Fund of The University of Alabama for support. Accordingly, the U.S.  
17  
18 Government retains a nonexclusive, royalty-free license to publish or reproduce the published form  
19  
20 of this contribution, or allow others to do so, for U.S. Government purposes.  
21  
22  
23  
24  
25  
26  
27  
28  
29  
30  
31  
32  
33  
34  
35  
36  
37  
38  
39  
40  
41  
42  
43  
44  
45  
46  
47  
48  
49  
50  
51  
52  
53  
54  
55  
56  
57  
58  
59  
60

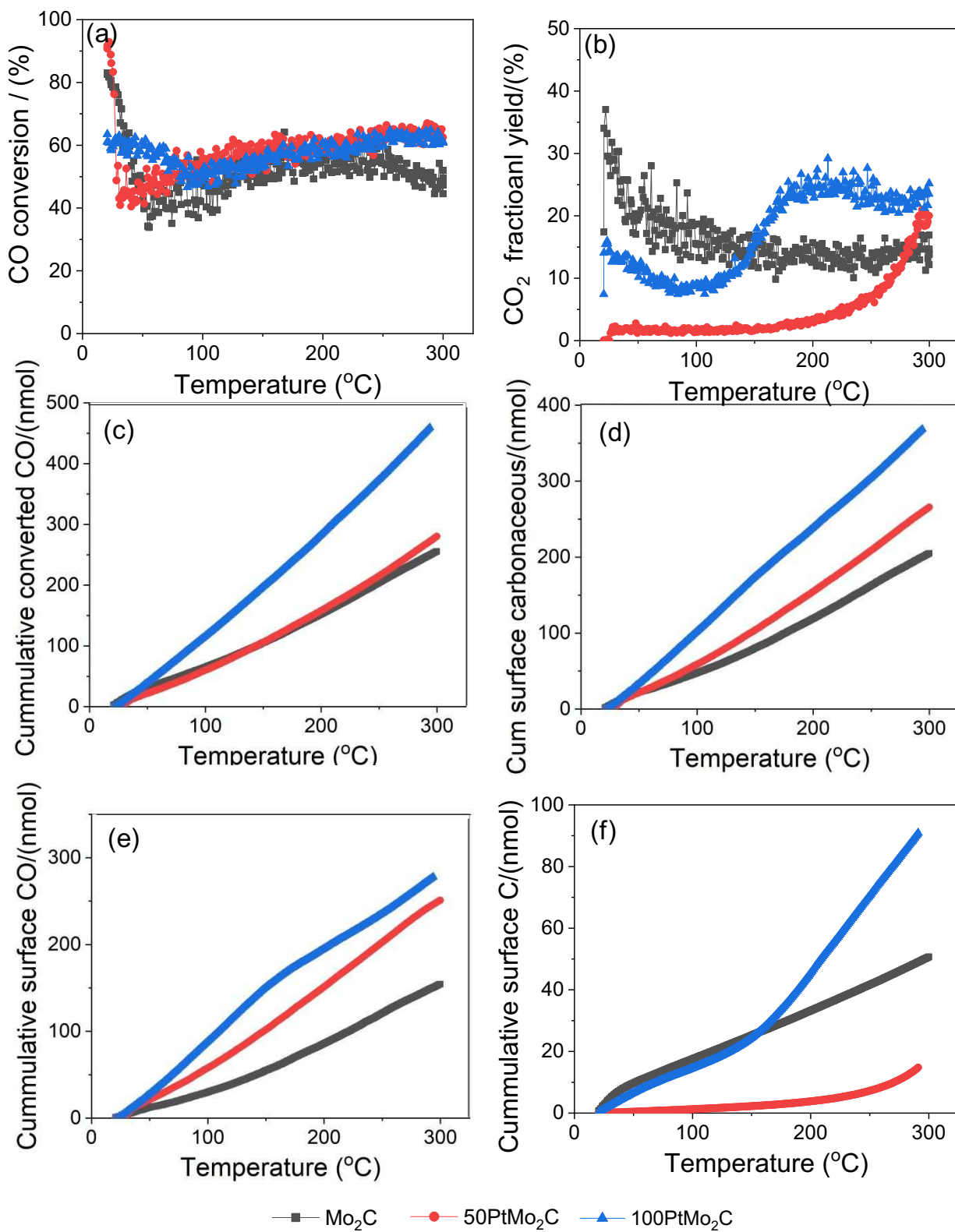
**Table 1.** Adsorption Energies in eV with the M06L and PBE Functionals ( $E_{\text{ads, M06L}}$  and  $E_{\text{ads, PBE}}$ ) and Optimized Bond Distances in Å for CO, C, O, and CO<sub>2</sub> Adsorption on Pt (111), Mo<sub>2</sub>C (100), and Pt/Mo<sub>2</sub>C Interface on the Most Stable Adsorption Sites with PBE.

Adsorbates	Site	$E_{\text{ads, M06L}}$	$E_{\text{ads, PBE}}$	$d_{\text{C-Pt}}$	$d_{\text{O-Pt}}$	$d_{\text{C-Mo}}$	$d_{\text{O-Mo}}$	$d_{\text{C-O}}$
Pt (111)								
1 <sup>st</sup> , CO	Top	-1.53	-1.69 <sup>h</sup>	1.841	-	-	-	1.152
2 <sup>nd</sup> , CO <sup>a</sup>	Top	-0.93	-1.04	1.858	-	-	-	1.150
C	FCC	-8.49	-7.34	1.899	-	-	-	-
O	FCC	-6.45	-4.53	-	2.049	-	-	-
CO <sub>2</sub> <sup>b</sup>	Top	-0.18	-0.24	3.973	-	-	-	1.174
$\beta$ -Mo <sub>2</sub> C (100)								
1 <sup>st</sup> , CO	UT	-2.19	-2.15	-	-	2.015	-	1.186
2 <sup>nd</sup> , CO <sup>a</sup>	UT	-2.18	-2.13	-	-	2.020	-	1.183
C <sup>c</sup>	LB	-10.23	-8.29	-	-	2.266	-	-
O	UB	-9.96	-7.89	-	-	-	1.955	-
CO <sub>2</sub> <sup>b,d</sup>	UT	-2.22	-2.43	-	-	2.226	2.194	1.127
Pt/Mo <sub>2</sub> C								
1 <sup>st</sup> , CO <sup>e</sup>	Pt, Top	-2.44	-2.27	1.848	-	-	-	1.161
2 <sup>nd</sup> , CO <sup>a,f</sup>	Mo, Top	-1.75	-1.82	2.093	-	2.156	-	1.181
C	Pt, Hollow	-8.92	-7.46	1.870	-	-	-	-
O	Mo, Bridge	-8.33	-5.81	1.907	-	-	2.041	-
CO <sub>2</sub> <sup>b,g</sup>	Mo, Top	-0.88	-0.84	1.926	-	2.472	2.163	1.297
						2.554	2.176	1.305

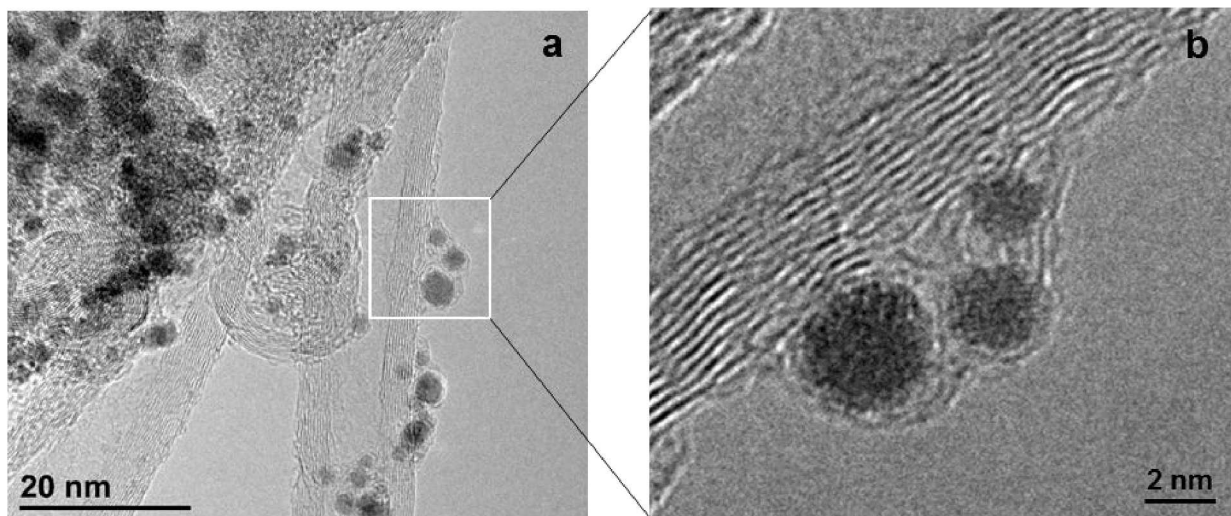
<sup>a</sup> CO adsorption energy on C and O preadsorbed surface; <sup>b</sup> CO<sub>2</sub> adsorption on C pre-adsorbed surface; <sup>c</sup> Bonded to a surface carbon with the C-C bond distance of 1.392 Å; <sup>d</sup>  $\angle$  O-C-O is 134.3°; <sup>e</sup>  $\angle$  Pt-C-O is 174.7°; <sup>f</sup>  $\angle$  Mo-C-Pt is 81.2° and  $\angle$  Mo-C-O is 151.1°. <sup>g</sup>  $\angle$  O-C-O is 122.8°; <sup>h</sup>The CO adsorption energy on a FCC site is predicted to be -1.79 eV with PBE.

1 **Table 2** Calculated Reaction Energies at 25°C ( $\Delta H_{298}$ , in eV) and Rate Constants ( $k$ , in s<sup>-1</sup>) from the Transition State Theory at 25, 100,  
 2 200, and 300 °C with both M06L and PBE Functionals. (g) Means the Reaction from the Gas Phases.

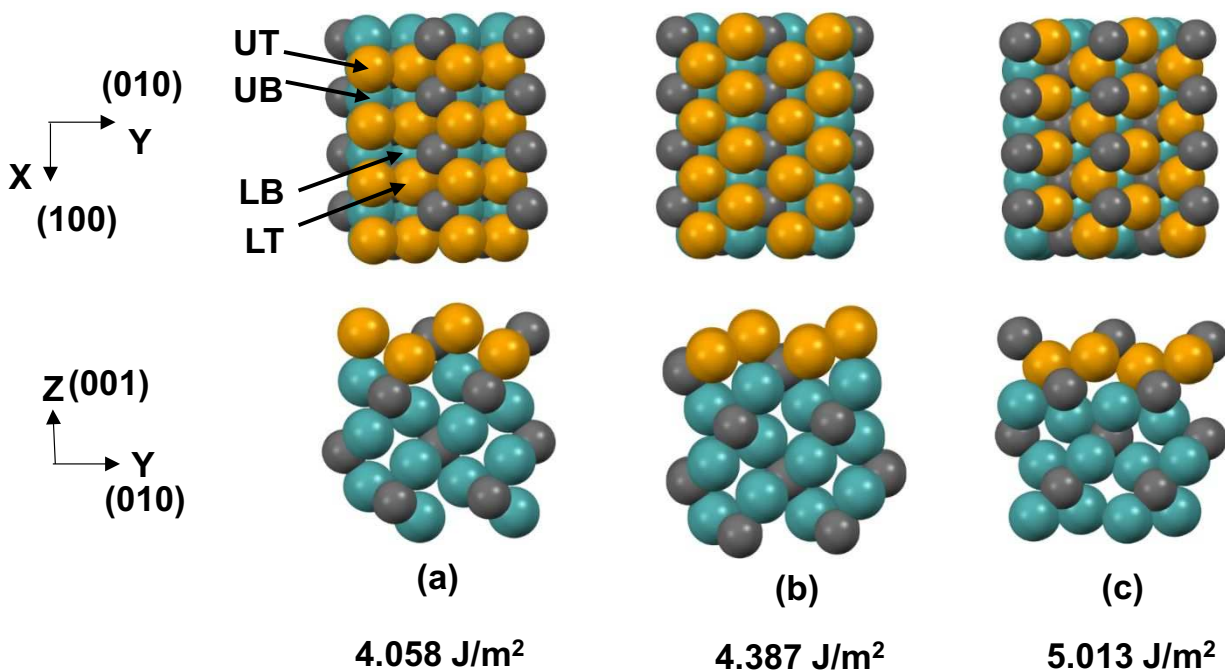
Reaction	M06L	$k$				PBE	$k$			
	$\Delta H_{298}$	25°C	100°C	200°C	300°C	$\Delta H_{298}$	25°C	100°C	200°C	300°C
$\beta$ -Mo <sub>2</sub> C (100)										
CO(g) + 2* → TS → C* + O*	-4.05	2.4x10 <sup>24</sup>	6.1x10 <sup>19</sup>	9.5x10 <sup>15</sup>	3.4x10 <sup>13</sup>	-3.91	5.1x10 <sup>23</sup>	1.8x10 <sup>19</sup>	3.6x10 <sup>16</sup>	1.7x10 <sup>14</sup>
CO(g) + C* + O* → TS → CO <sub>2</sub> * + C*	-1.27	3.6x10 <sup>7</sup>	3.0x10 <sup>6</sup>	4.0x10 <sup>5</sup>	1.2x10 <sup>5</sup>	-1.20	3.6x10 <sup>10</sup>	1.4x10 <sup>9</sup>	8.6x10 <sup>7</sup>	1.6x10 <sup>7</sup>
CO* + * → TS → C* + O*	-1.90	1.4x10 <sup>-1</sup>	5.8x10 <sup>1</sup>	9.1x10 <sup>3</sup>	2.5x10 <sup>5</sup>	-1.80	1.4x10 <sup>-1</sup>	5.6x10 <sup>1</sup>	8.9x10 <sup>3</sup>	2.4x10 <sup>5</sup>
CO* + C* + O* → TS → CO <sub>2</sub> * + C* + *	0.88	2.7x10 <sup>-18</sup>	3.5x10 <sup>-12</sup>	4.6x10 <sup>-7</sup>	9.9x10 <sup>-4</sup>	0.89	2.9x10 <sup>-15</sup>	9.2x10 <sup>-10</sup>	3.7x10 <sup>-5</sup>	3.7x10 <sup>-2</sup>
Pt/Mo <sub>2</sub> C										
CO(g) + 2* <sub>Mo</sub> → TS → C* <sub>Mo</sub> + O* <sub>Mo</sub>	-0.69	3.3x10 <sup>1</sup>	3.5x10 <sup>1</sup>	4.2x10 <sup>1</sup>	5.2x10 <sup>1</sup>	-0.40	8.2x10 <sup>-3</sup>	4.7x10 <sup>-2</sup>	2.3x10 <sup>-1</sup>	7.0x10 <sup>-1</sup>
CO(g) + C* <sub>Mo</sub> + O* <sub>Mo</sub> → TS → CO <sub>2</sub> * <sub>Mo</sub> + C* <sub>Mo</sub>	-1.82	1.1x10 <sup>15</sup>	3.1x10 <sup>12</sup>	2.5x10 <sup>10</sup>	1.2x10 <sup>9</sup>	-1.69	8.7x10 <sup>15</sup>	1.6x10 <sup>13</sup>	9.3x10 <sup>10</sup>	3.5x10 <sup>9</sup>
CO* <sub>Mo</sub> + * → TS → C* <sub>Mo</sub> + O* <sub>Mo</sub>	0.96	9.3x10 <sup>-16</sup>	2.6x10 <sup>-10</sup>	1.0x10 <sup>-5</sup>	1.0x10 <sup>-2</sup>	0.96	6.3x10 <sup>-15</sup>	1.2x10 <sup>-9</sup>	3.4x10 <sup>-5</sup>	2.7x10 <sup>-2</sup>
CO* <sub>Mo</sub> + C* <sub>Mo</sub> + O* <sub>Mo</sub> → TS → CO <sub>2</sub> * <sub>Mo</sub> + C* <sub>Mo</sub> + * <sub>Mo</sub>	-0.08	2.5x10 <sup>-3</sup>	4.8x10 <sup>0</sup>	2.8x10 <sup>3</sup>	1.8x10 <sup>5</sup>	0.12	1.4x10 <sup>-3</sup>	3.0x10 <sup>0</sup>	2.0x10 <sup>3</sup>	1.4x10 <sup>5</sup>
CO* <sub>Pt</sub> → TS → CO* <sub>Mo</sub>	0.74	9.9x10 <sup>-3</sup>	8.1x10 <sup>0</sup>	2.3x10 <sup>3</sup>	9.2x10 <sup>4</sup>	0.85	2.8x10 <sup>-4</sup>	4.8x10 <sup>-1</sup>	2.5x10 <sup>2</sup>	1.5x10 <sup>4</sup>
C* <sub>Mo</sub> → TS → C* <sub>Pt</sub>	-0.18	5.3x10 <sup>-3</sup>	6.1x10 <sup>0</sup>	2.3x10 <sup>3</sup>	1.8x10 <sup>5</sup>	-0.62	5.3x10 <sup>-1</sup>	1.5x10 <sup>3</sup>	1.8x10 <sup>5</sup>	3.9x10 <sup>6</sup>
Pt (111)										
CO(g) + 2* → TS → C* + O*	1.26	1.3x10 <sup>-45</sup>	2.7x10 <sup>-36</sup>	1.9x10 <sup>-28</sup>	2.8x10 <sup>-23</sup>	0.43	2.3x10 <sup>-31</sup>	6.4x10 <sup>-25</sup>	1.8x10 <sup>-19</sup>	7.1x10 <sup>-16</sup>
CO(g) + C* + O* → TS → CO <sub>2</sub> * + C*	-2.77	2.8x10 <sup>14</sup>	9.5x10 <sup>11</sup>	8.8x10 <sup>9</sup>	4.5x10 <sup>8</sup>	-2.39	1.1x10 <sup>15</sup>	2.8x10 <sup>12</sup>	2.0x10 <sup>10</sup>	9.1x10 <sup>8</sup>
CO* + * → TS → C* + O*	2.73	9.3x10 <sup>-60</sup>	1.5x10 <sup>-45</sup>	1.3x10 <sup>-33</sup>	7.8x10 <sup>-26</sup>	2.06	2.7x10 <sup>-48</sup>	2.1x10 <sup>-36</sup>	2.1x10 <sup>-26</sup>	7.1x10 <sup>-20</sup>
CO* + C* + O* → TS → CO <sub>2</sub> * + C* + *	-1.31	2.1x10 <sup>0</sup>	5.8x10 <sup>2</sup>	6.4x10 <sup>4</sup>	1.4x10 <sup>6</sup>	-0.83	3.7x10 <sup>-1</sup>	1.4x10 <sup>2</sup>	2.2x10 <sup>4</sup>	5.6x10 <sup>5</sup>

4  
5

1  
2  
3 **Figure 1.** (a) CO Conversion, (b) CO<sub>2</sub> Fractional Yield, (c) Cumulative Converted CO ( $N_{\text{converted}}$ ,  
4 Adsorption + Reaction), (d) Cumulative Surface Carbonaceous Species ( $N_{\text{carb}} = N_{\text{CO}} + N_{\text{C}}$ ), (e)  
5  
6 Cumulative Surface CO ( $N_{\text{CO}}$ ) and (f) Cumulative Surface C ( $N_{\text{C}}$ , the C atoms from the  
7  
8 Boudouard process only) During CO Pulsing over the Mo<sub>2</sub>C and Pt/Mo<sub>2</sub>C Catalysts While  
9  
10 Heating up to 300 °C at 1 °C/min. (a) and (b) are reprinted with permission from Tan, S.; Wang,  
11  
12 L.; Saha, S.; Fushimi, R. R.; Li, D. Active Site and Electronic Structure Elucidation of Pt  
13  
14 Nanoparticles Supported on Phase-Pure Molybdenum Carbide Nanotubes. *ACS Appl. Mater.*  
15  
16 *Interfaces* **2017**, *9*, 9815–9822. Copyright 2017 American Chemical Society.  
17  
18  
19  
20  
21  
22  
23  
24  
25  
26  
27  
28  
29  
30  
31  
32  
33  
34  
35  
36  
37  
38  
39  
40  
41  
42  
43  
44  
45  
46  
47  
48  
49  
50  
51  
52  
53  
54  
55  
56  
57  
58  
59  
60



17  
18 **Figure 2.** (a) TEM and (b) High-resolution TEM images of 100 Pt/Mo<sub>2</sub>C Catalyst After  
19 Temperature Programmed Reaction with CO Pulses.  
20  
21  
22  
23  
24  
25  
26  
27  
28  
29  
30  
31  
32  
33  
34  
35  
36  
37  
38  
39  
40  
41  
42  
43  
44  
45  
46  
47  
48  
49  
50  
51  
52  
53  
54  
55  
56  
57  
58  
59  
60



28  
29  
30  
31  
32  
33  
34  
35  
36  
37  
38  
39  
40  
41  
42  
43  
44  
45  
46  
47  
48  
49  
50  
51  
52  
53  
54  
55  
56  
57  
58  
59  
60

**Figure 3.** Top and Side View of (a) Most Stable Mo-Terminated Surface, (b) A Second Mo-Terminated Surface, and (c) C-Terminated Surface for  $\beta$ - $\text{Mo}_2\text{C}$  (100). The Cleavage Energies Are Shown Below with the M06L Functional. Five Different Adsorption Sites: Upper Top (UT), Upper Bridge (UB), Lower Top (LT), and Lower Bridge (LB) on the Most Stable Mo-Terminated Surface (a). C Atoms Shown in Grey and Mo Atoms Shown in Steel Blue. For Clarity, the First Layer Mo Atoms are shown in Orange.

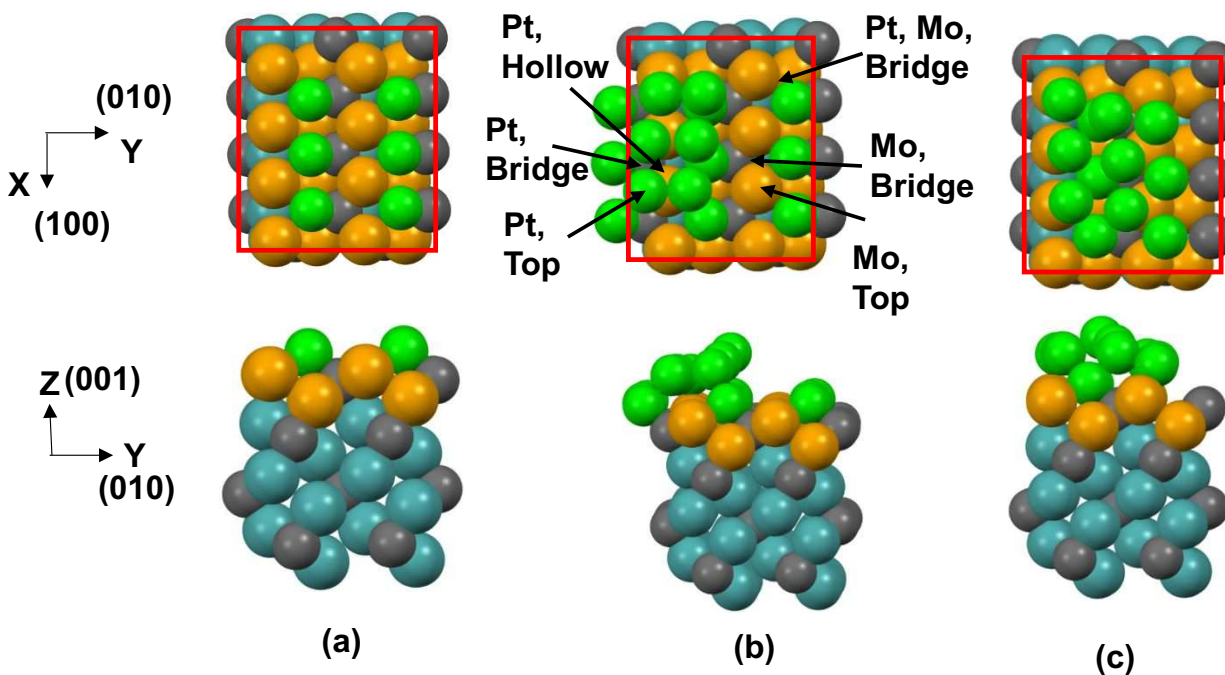
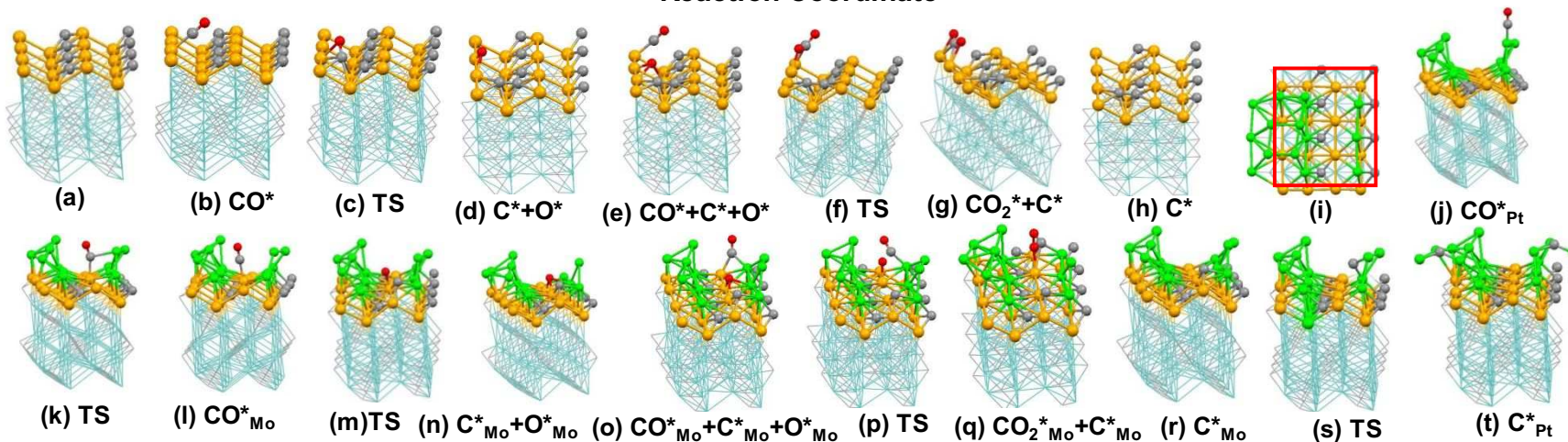
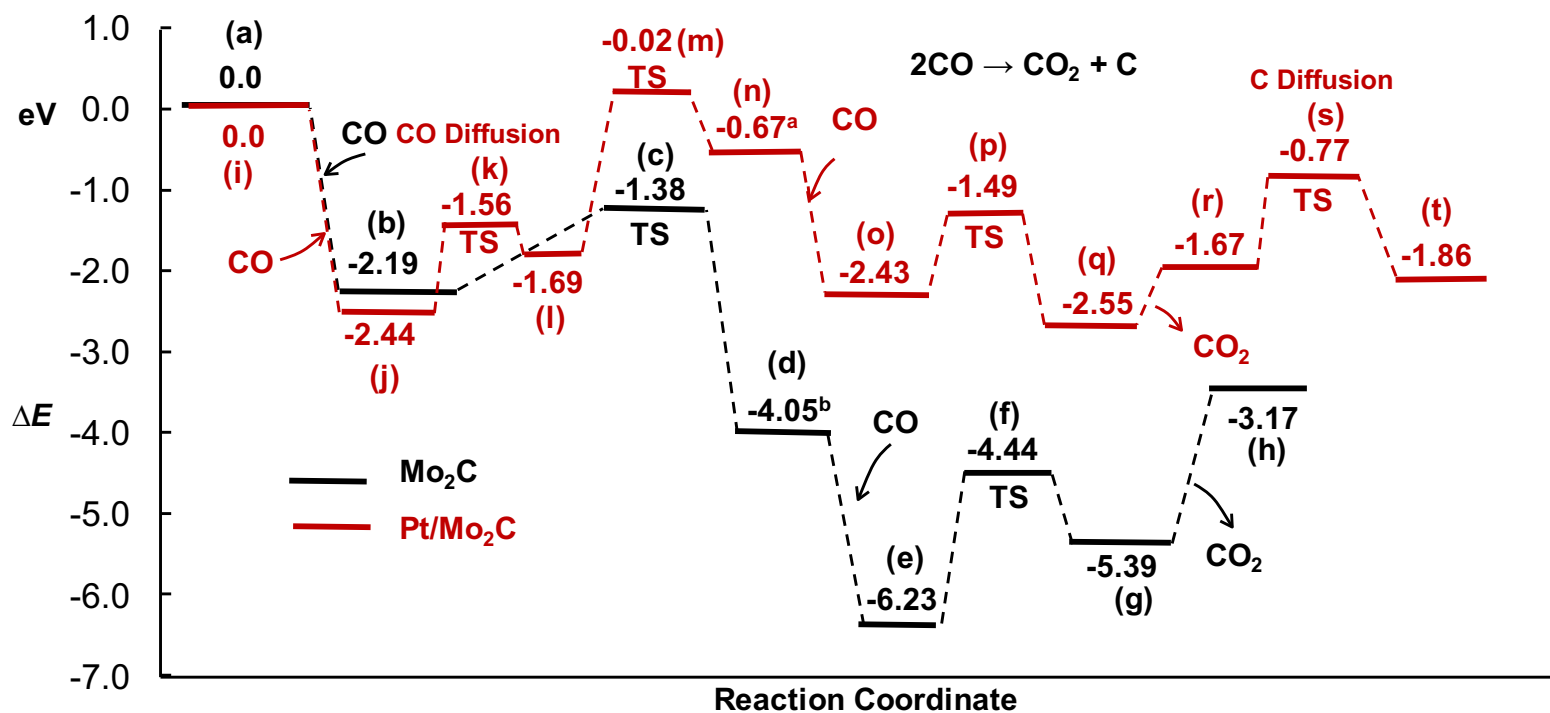


**Figure 4.** Top and Side View of (a) Most Stable 6Pt@Mo<sub>2</sub>C Surface, (b) Most Stable 12Pt@Mo<sub>2</sub>C Interface, and (c) a Second 12Pt@Mo<sub>2</sub>C Interface. C Atoms Shown in Grey, Mo Atoms Shown in Blue and Pt Atoms Shown in Green. For Clarity, the First Layer Mo Atoms are shown in Orange.



1  
2  
3 **Figure 5.** Potential Energy Surface for Boudouard Reaction  $2\text{CO} \rightarrow \text{CO}_2 + \text{C}$  on Pure  $\beta\text{-Mo}_2\text{C}$  (100) Surface and Pt/ $\text{Mo}_2\text{C}$  (100)  
4 Interface at 0 K with M06L. <sup>a</sup> Dissociation Energy Calculated from Independent Pt/ $\text{Mo}_2\text{C}$  (100)-C and Pt/ $\text{Mo}_2\text{C}$  (100)-O Calculations  
5 is -1.24 eV. <sup>b</sup> Dissociation Energy Calculated from Independent  $\text{Mo}_2\text{C}$  (100)-C and  $\text{Mo}_2\text{C}$  (100)-O Calculations is -4.36 eV. Oxygen  
6  
7  
8 Atoms Shown in Red and See Figure 3 and 4 Captions for the Colors of the Other Atoms.  
9  
10  
11  
12  
13  
14  
15  
16  
17  
18  
19  
20  
21  
22  
23  
24  
25  
26  
27  
28  
29  
30  
31  
32  
33  
34  
35  
36  
37  
38  
39  
40  
41  
42  
43  
44  
45  
46  
47

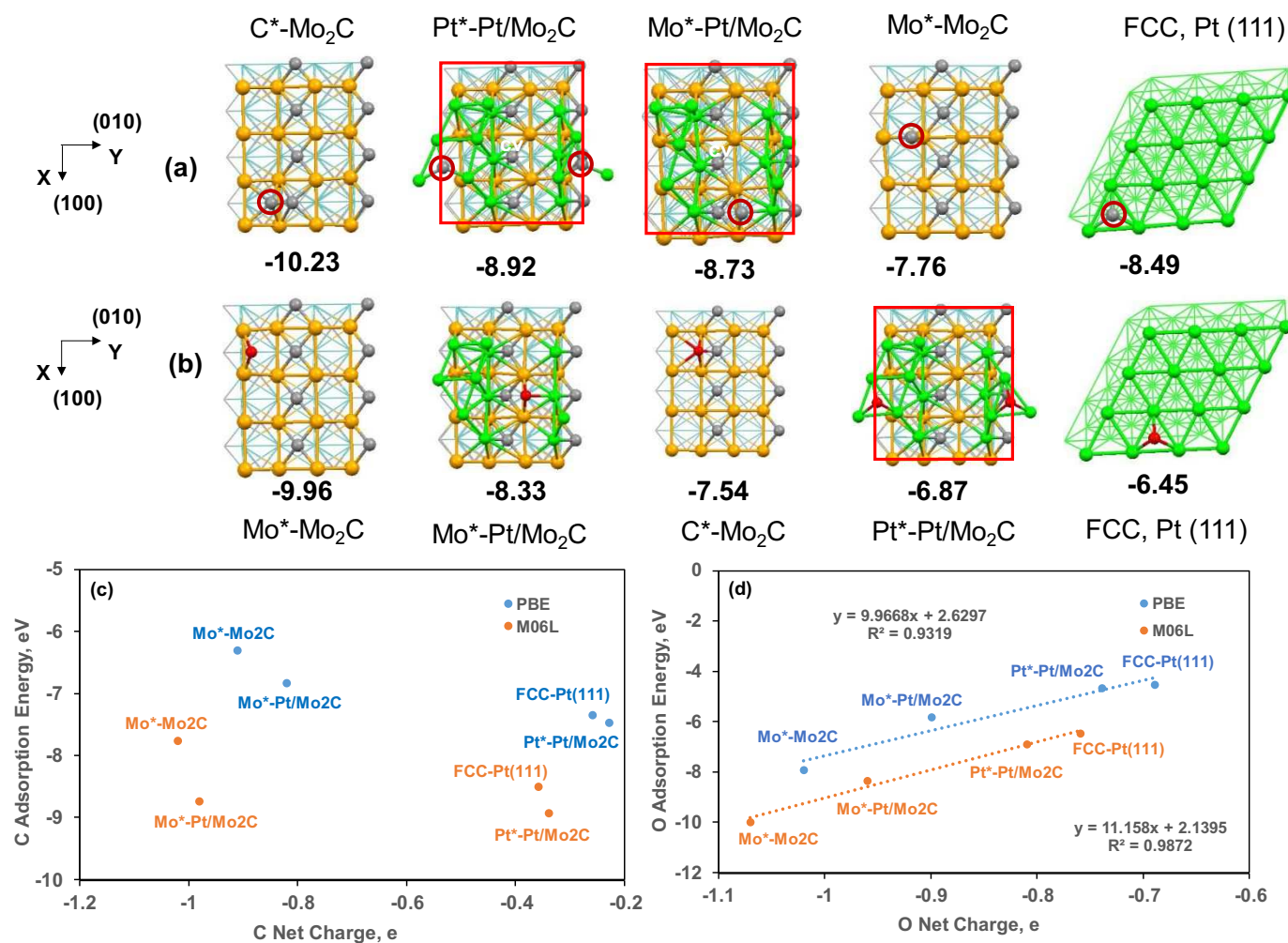


**Figure 6.** Adsorption Energies of C (a) and O (b) on Different Sites of the Most Stable Mo-Terminated  $\beta$ - $\text{Mo}_2\text{C}$  (100) and Pt/Mo $_2\text{C}$  Interface in eV with M06L; The Correlation Between the Adsorption Energies and the Net Charges of the Adsorbates for C (c) and O (d).

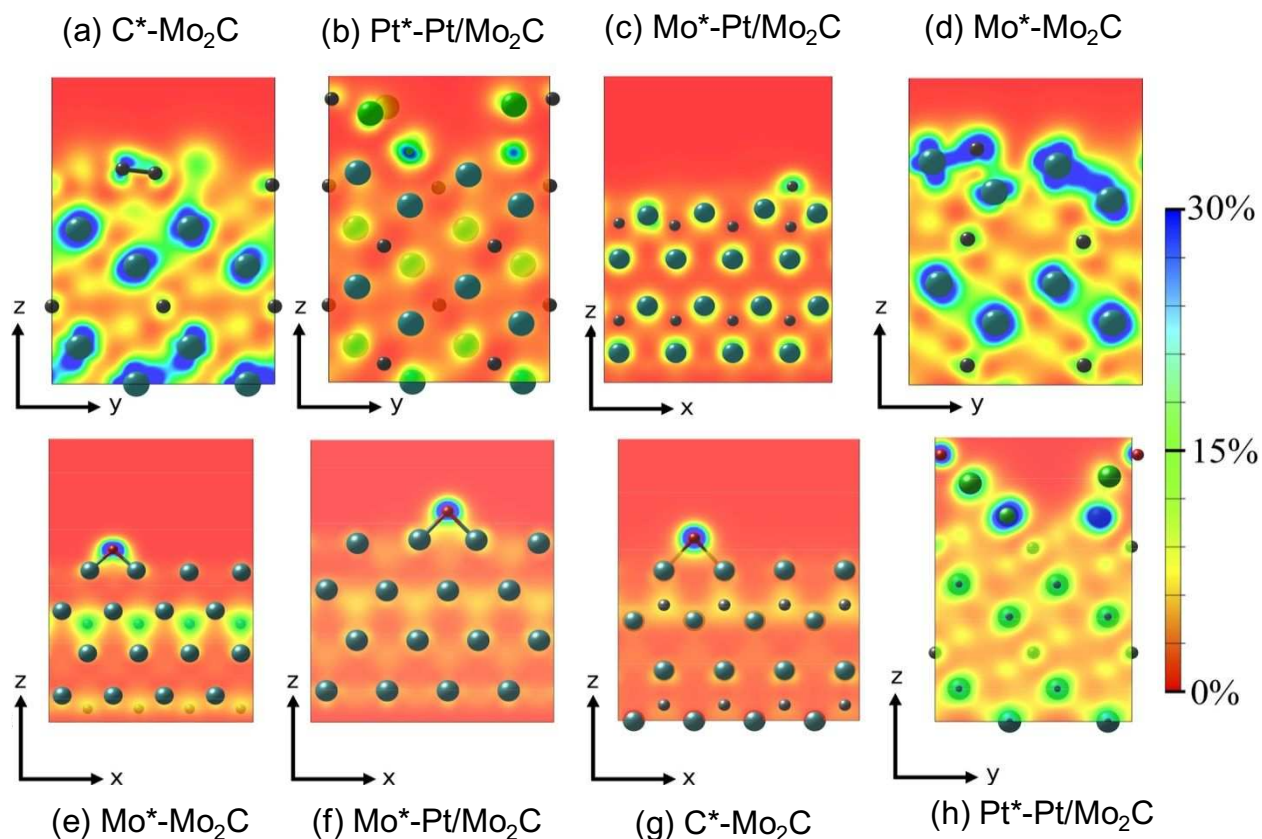


**Figure 7.** Cross Sections of the Partial Charge Density of C from -2 eV to the Fermi energy (a-d) and O from -8 eV to -5 eV (e-h) on Different Sites of the Most Stable Mo-Terminated  $\beta$ - $\text{Mo}_2\text{C}$  (100) and Pt/ $\text{Mo}_2\text{C}$  Interface. The Energy Range Has Been Narrowed to 30% of the Total Electronic States to Improve Bond Visibility. Red Represents No Density of States While Blue Represents the Most Density of States. C, Mo, O, and Pt Atoms are Shown in Dark Grey, Steel Blue, Red, and Green Respectively. In Figures c and f, the Bonding of the Adsorbate with Both Mo and Pt Cannot be Seen in One Plane.

1  
2  
3 **Supporting Information.** DRIFTS experiment shows CO<sub>2</sub> peaks on Pt/Mo<sub>2</sub>C; Derivation of  
4 transient pressure; Number of surface atoms estimation; Free energy and rate constant calculations;  
5  
6 Detailed description of CO on Pt (111); Figures: DRIFT spectra; Transient pressure at different  
7  
8 temperatures; TPD spectra before pulsing experiment; TPD spectra with CO preadsorption; EDX  
9  
10 analysis after pulsing experiment; Calculated potential energy surfaces and free energy surfaces;  
11  
12 CO<sub>2</sub>, C and O adsorptions on Pt(111), β-Mo<sub>2</sub>C(100), and Pt/Mo<sub>2</sub>C surfaces; DOS and ELF for C  
13  
14 and O adsorption structures; Tables: Bader charge analysis for CO, CO<sub>2</sub>, C, and O adsorption  
15  
16 structures. This material is available free of charge via the internet at <http://pubs.acs.org>.  
17  
18  
19  
20  
21  
22  
23  
24  
25  
26  
27  
28  
29  
30  
31  
32  
33  
34  
35  
36  
37  
38  
39  
40  
41  
42  
43  
44  
45  
46  
47  
48  
49  
50  
51  
52  
53  
54  
55  
56  
57  
58  
59  
60

## References

- <sup>1</sup> Huang, S.-C.; Lin, C.-H.; Wang, J.-H. Trends of Water Gas Shift Reaction on Close-Packed Transition Metal Surfaces. *J. Phys. Chem. C* **2010**, *114*, 9826–9834.
- <sup>2</sup> Gao, J.; Liu, Q.; Gu, F.; Liu, B.; Zhong, Z.; Su, F. Recent Advances in Methanation Catalysts for the Production of Synthetic Natural Gas. *RSC Adv.* **2015**, *5*, 22759–22776
- <sup>3</sup> Schaidle, J. A.; Thompson, L. T. Fischer-Tropsch Synthesis over Early Transition Metal Carbides and Nitrides: CO Activation and Chain Growth. *J. Catal.* **2015**, *329*, 325–334.
- <sup>4</sup> Tian, X.; Wang, T.; Jiao, H. Mechanism of Coverage Dependent CO Adsorption and Dissociation on the Mo (100) Surface. *Phys. Chem. Chem. Phys.* **2017**, *19*, 2186–2192
- <sup>5</sup> Morikawa, Y.; Mortensen, J. J.; Hammer, B.; Norskov, J. K. CO Adsorption and Dissociation on Pt(111) and Ni(111) Surfaces. *Surf. Sci.* **1997**, *386*, 67-72.
- <sup>6</sup> Hwu, H. H.; Chen, J. G. Surface Chemistry of Transition Metal Carbides. *Chem. Rev.* **2005**, *105*, 185–212.
- <sup>7</sup> Posada-Pérez, S.; Vines, F.; Ramirez, P. J.; Vidal, A. B.; Rodriguez, J. A.; Illas, F. The Bending Machine: CO<sub>2</sub> Activation and Hydrogenation on  $\delta$ -MoC(001) and  $\beta$ -Mo<sub>2</sub>C(001) Surfaces. *Phys. Chem. Chem. Phys.* **2014**, *16*, 14912– 14921.
- <sup>8</sup> Posada-Perez, S.; Ramírez, P. J.; Gutierrez, R. A.; Stacchiola, D. J.; Viñ es, F.; Liu, P.; Illas, F.; Rodriguez, J. A. The Conversion of CO<sub>2</sub> to Methanol on Orthorhombic  $\beta$ -Mo<sub>2</sub>C and Cu/ $\beta$ -Mo<sub>2</sub>C Catalysts: Mechanism for Admetal Induced Change in the Selectivity and Activity. *Catal. Sci. Technol.* **2016**, *6*, 6766–6777
- <sup>9</sup> Xiang, M.; Wu, D.; Zou, J.; Li, D.; Sun, Y.; She, X. Catalytic performance of Fe modified K/MO<sub>2</sub>C catalyst for CO hydrogenation. *J. Nat. Gas Chem.* **2011**, *20*, 520-524

- 1  
2  
3  
4 <sup>10</sup> Tan, S.; Wang, L.; Saha, S.; Fushimi, R. R.; Li, D. Active Site and Electronic Structure  
5  
6 Elucidation of Pt Nanoparticles Supported on Phase-Pure Molybdenum Carbide Nanotubes. *ACS*  
7  
8 *Appl. Mater. Interfaces* **2017**, *9*, 9815–9822  
9  
10  
11 <sup>11</sup> Schweitzer, N. M.; Schaidle, J. A.; Ezekoye, O. K.; Pan, X.; Linic, S.; Thompson, L. T. High  
12  
13 Activity Carbide Supported Catalysts for Water Gas Shift. *J. Am. Chem. Soc.* **2011**, *133*,  
14  
15 2378–2381.  
16  
17  
18 <sup>12</sup> Schweitzer, N. M.; Schaidle, J. A.; Ezekoye, Q. K.; Pan, X.; Linic, S.; Thompson, L. T. High  
19  
20 Activity Carbide Supported Catalysts for Water Gas Shift. *J. Am. Chem. Soc.* **2011**, *133*,  
21  
22 2378–2381.  
23  
24  
25 <sup>13</sup> Moon, D. J.; Ryu, J. W. Molybdenum Carbide Water–Gas Shift Catalyst for Fuel Cell-  
26  
27 Powered Vehicles Applications. *Catal. Lett.* **2004**, *92*, 17–24  
28  
29  
30 <sup>14</sup> Yao, S. Y.; Zhang, X.; Zhou, W.; Gao, R.; Xu, W. Q.; Ye, Y. F.; Lin, L. L.; Wen, X. D.; Liu,  
31  
32 P.; Chen, B. B.; Crumlin, E.; Guo, J. H.; Zuo, Z. J.; Li, W. Z.; Xie, J. L.; Lu, L.; Kiely, C. J.; Gu,  
33  
34 L.; Shi, C.; Rodriguez, J. A.; Ma, D. Atomic-Layered Au Clusters on Alpha-MoC as Catalysts  
35  
36 for the Low-Temperature Water-Gas Shift Reaction. *Science* **2017**, *357*, 389–393.  
37  
38  
39 <sup>15</sup> Zhang, X.; Zhu, X.; Lin, L.; Yao, S.; Zhang, M.; Liu, X.; Wang, X.; Li, Y.-W.; Shi, C.; Ma, D.  
40  
41 Highly Dispersed Copper over  $\beta$ -Mo<sub>2</sub>C as an Efficient and Stable Catalyst for the Reverse Water  
42  
43 Gas Shift (RWGS) Reaction. *ACS Catal.* **2017**, *7*, 912–918.  
44  
45  
46 <sup>16</sup> Rodriguez, J. A.; Liu, P.; Stacchiola, D. J.; Senanayake, S. D.; White, M. G.; Chen, J. G.  
47  
48 Hydrogenation of CO<sub>2</sub> to Methanol: Importance of Metal–Oxide and Metal–Carbide Interfaces  
49  
50 in the Activation of CO<sub>2</sub>. *ACS Catal.* **2015**, *5*, 6696–6706.  
51  
52  
53  
54  
55  
56  
57  
58  
59  
60

- 1  
2  
3  
4  
5  
6  
7  
8  
9  
10  
11  
12  
13  
14  
15  
16  
17  
18  
19  
20  
21  
22  
23  
24  
25  
26  
27  
28  
29  
30  
31  
32  
33  
34  
35  
36  
37  
38  
39  
40  
41  
42  
43  
44  
45  
46  
47  
48  
49  
50  
51  
52  
53  
54  
55  
56  
57  
58  
59  
60
- 
- <sup>17</sup> Rodriguez, J. A.; Illas, F. Activation of Noble Metals on Metal-Carbide Surfaces: Novel Catalysts for CO oxidation, Desulfurization and Hydrogenation Reactions. *Phys. Chem. Chem. Phys.* **2012**, *14*, 427–438.
- <sup>18</sup> Rodriguez, J. A.; Evans, J.; Feria, L.; Vidal, A. B.; Liu, P.; Nakamura, K.; Illas, F. CO<sub>2</sub> hydrogenation on Au/TiC, Cu/TiC, and Ni/TiC catalysts: Production of CO, methanol, and methane. *J. Catal.* **2013**, *307*, 162–163.
- <sup>19</sup> H. Prats, R. A. Gutiérrez, J. J. Piñero, F. Viñes, S. T. Bromley, P. J. Ramírez, J. A. Rodríguez and F. Illas, Room Temperature Methane Capture and Activation by Ni Clusters Supported on TiC (001): Effects of Metal–Carbide Interactions on the Cleavage of the C–H Bond. *J. Am. Chem. Soc.*, 2019, **141**, 5303–5313
- <sup>20</sup> Koverga, A. A.; Florez, E.; Dorkis, L.; Rodriguez, J. A. CO, CO<sub>2</sub>, and H<sub>2</sub> interactions with (0001) and (001) Tungsten Carbide Surfaces : Importance of Carbon and Metal Sites. *J. Phys. Chem. C*, **2019**, *123*, 8871–8883.
- <sup>21</sup> Wang, T.; Li, Y. W.; Wang, J.; Beller, M.; Jiao, H. High Coverage CO Adsorption and Dissociation on the Orthorhombic Mo<sub>2</sub>C(100) Surface. *J. Phys. Chem. C* **2014**, *118*, 3162-3171.
- <sup>22</sup> Wang, T.; Luo, Q.; Li, Y.-W. W.; Wang, J.; Beller, M.; Jiao, H. Stable Surface Terminations of Orthorhombic Mo<sub>2</sub>C Catalysts and Their CO Activation Mechanisms. *Appl. Catal., A* **2014**, *478*, 146–156.
- <sup>23</sup> Wang, T.; Liu, X. W.; Wang, S. G.; Huo, C. F.; Li, Y. W.; Wang, J. G.; Jiao, H. Stability of β-Mo<sub>2</sub>C Facets from ab Initio Atomistic Thermodynamics. *J. Phys. Chem. C* **2011**, *115*, 22360–22368.

- 1  
2  
3  
4 24 Pistonesi, C.; Pronsato, M. E.; Bugyi, L.; Juan, A. Theoretical Model for CO Adsorption and  
5  
6  
7 Dissociation on Clean and K-Doped  $\beta$ -Mo<sub>2</sub>C Surfaces. *J. Phys. Chem. C* **2012**, *116*,  
8  
9 24573–24581  
10  
11 25 Zhao, Y.; Li, S.; Sun, Y. Ni-Doping Effects on Carbon Diffusion and Oxidation over Mo<sub>2</sub>C  
12  
13 Surfaces. *J. Phys. Chem. C* **2013**, *117*, 18936–18946.  
14  
15  
16 26 Shi, Y.; Yang, Y.; Li, Y. W.; Jiao, H. Activation Mechanisms of H<sub>2</sub>, O<sub>2</sub>, H<sub>2</sub>O, CO<sub>2</sub>, CO, CH<sub>4</sub>  
17  
18 and C<sub>2</sub>H<sub>x</sub> on Metallic Mo<sub>2</sub>C(001) as Well as Mo/C Terminated Mo<sub>2</sub>C(101) from Density  
19  
20 Functional Theory Computations. *Appl. Catal., A* **2016**, *524*, 223–236.  
21  
22  
23 27 Gleaves, J. T.; Yablonsky, G. S.; Phanawadee, P.; Schuurman, Y. TAP-2: An interrogative  
24  
25 kinetics approach. *Appl. Catal. A* **1997**, *160*, 55–88  
26  
27  
28 28 Morgan, K.; Maguire, N.; Fushimi, R.; Gleaves, J.T.; Goguet, A.; Harold, M.P.; Kondratenko,  
29  
30 E.V.; Menon, U.; Schuurman, Y.; Yablonsky, G.S. Forty years of temporal analysis of products.  
31  
32 *Catal. Sci. Tech.* **2017**, *7*, 2416-2439  
33  
34  
35 29 Saha, S.; Martin, B.; Leonard, B.; Li, D. Probing synergetic effects between platinum  
36  
37 nanoparticles deposited via atomic layer deposition and molybdenum carbide nanotube support  
38  
39 through surface characterization and device performance. *J. Mater. Chem. A*, **2016**, *4*, 9253-  
40  
41 9265.  
42  
43  
44 30 Chen, J. Carbide and Nitride Overlayers on Early Transition Metal Surfaces: Preparation,  
45  
46 Characterization, and Reactivities. *Chem. Rev.* **1996**, *96*, 1447-1498.  
47  
48  
49 31 Perdew, J. P.; Burke, K.; Ernzerhof, M. Generalized Gradient Approximation Made Simple.  
50  
51 *Phys. Rev. Lett.* **1996**, *77*, 3865–3868. *Errata. Phys. Rev. Lett.* **1997**, *78*, 1396.  
52  
53  
54 32 Kresse, G.; Furthmüller, J. Efficiency of Ab-Initio Total Energy Calculations for Metals and  
55  
56 Semiconductors Using a Plane-Wave Basis Set. *Comput. Mater. Sci.* **1996**, *6*, 15–50.  
57  
58  
59  
60

- 1  
2  
3  
4 33 Kresse, G.; Hafner, J. Ab Initio Molecular Dynamics for Open- Shell Transition Metals. *Phys.*  
5 *Rev. B* **1993**, *48*, 13115–13118  
6  
7  
8  
9 34 Kresse, G.; Hafner, J. Ab Initio Molecular Dynamics for Liquid Metals. *Phys. Rev. B* **1993**, *47*,  
10 558–561.  
11  
12  
13 35 Kresse, G.; Joubert, D. From Ultrasoft Pseudopotentials to the Projector Augmented-Wave  
14 Method. *Phys. Rev. B* **1999**, *59*, 1758– 1775.  
15  
16  
17  
18 36 Blochl, P. E. Projector Augmented-Wave Method. *Phys. Rev. B* **1994**, *50*, 17953–17979  
19  
20 37 Luo, S.; Zhao, Y.; Truhlar, D. G. Improved CO Adsorption Energies, Site Preferences, and  
21 Surface Formation Energies from a Meta-Generalized Gradient Approximation Exchange–  
22 Correlation Functional, M06-L. *J. Phys. Chem. Lett.* **2012**, *3*, 2975-2979.  
23  
24  
25  
26 38 Alaei, M.; Akbarzadeh, H.; Gholizadeh, H.; de Gironcoli, S. CO/ Pt(111): GGA Density  
27 Functional Study of Site Preference for Adsorption. *Phys. Rev. B* **2008**, *77*, 085414.  
28  
29  
30 39 Janthon, P.; Viñ es, F.; Sirijaraensre, J.; Limtrakul, J.; Illas, F. Adding Pieces to the  
31 CO/Pt(111) Puzzle: The Role of Dispersion. *J. Phys. Chem. C* **2017**, *121*, 3970–3977  
32  
33  
34 40 Zhao, Y.; Truhlar, D. G. A new Local Density Functional for Main-Group Thermochemistry,  
35 Transition Metal Bonding, Thermochemical Kinetics, and Noncovalent Interactions. *J. Chem.*  
36 *Phys.* **2006**, *125*, 194101 (18 pages).  
37  
38  
39 41 Singh-Miller, N. E.; Marzari, N. Surface Energies, Work Functions, and Surface Relaxations  
40 of Low Index Metallic Surfaces from First-Principles. *Phys. Rev. B* **2009**, *80*, 235407.  
41  
42  
43 42 Kittel, C. *Introduction to Solid State Physics*, 7th ed.; John Wiley and Sons: New York, 1976.  
44  
45  
46 43 Dubois, J.; Epicier, T.; Esnouf, C.; Fantozzi, G.; Convert, P. Neutron powder diffraction  
47 studies of transition metal hemicarbides  $M_2C_{1-x}$ . I. Motivation for a study on  $W_2C$  and  $Mo_2C$  and  
48  
49  
50  
51  
52  
53  
54  
55  
56  
57  
58  
59  
60

Experimental Background for an in situ Investigation at Elevated Temperature. *Acta Metall.*

**1988**, *8*, 1891-1901

<sup>44</sup> Epicier, T.; Dubois, J.; Esnouf, C.; Fantozzi, G.; Convert, P. Neutron powder diffraction studies of transition metal hemicarbides  $M_2C_{1-x}$ . In situ high temperature study on  $W_2C_{1-x}$  and  $Mo_2C_{1-x}$ . *Acta Metall.* **1988**, *8*, 1903-1921.

<sup>45</sup> Politi, J. R. d. S.; Vines, F.; Rodriguez, J. A.; Illas, F. Atomic and Electronic Structure of Molybdenum Carbide Phases: Bulk and Low Miller-Index Surfaces. *Phys. Chem. Chem. Phys.* **2013**, *15*, 12617– 12625.

<sup>46</sup> Haines, J.; Leger, J. M.; Chateau, C.; Lowther, J. E. Experimental and Theoretical Investigation of  $Mo_2C$  at High Pressure. *J. Phys.: Condens. Matter* **2001**, *13*, 2447-2454.

<sup>47</sup> Han, J. W.; Li, L. W.; Sholl, D. S. Density Functional Theory Study of H and CO Adsorption on Alkali-Promoted  $Mo_2C$  Surfaces. *J. Phys. Chem. C* **2011**, *115*, 6870–6876

<sup>48</sup> Shi, X. R.; Wang, S. G.; Wang, H.; Deng, C. M.; Qin, Z. F.; Wang, J. Structure and stability of  $\beta$ - $Mo_2C$  bulk and surfaces: A density functional theory study. *Surf. Sci.* **2009**, *603*, 852-859.

<sup>49</sup> Rudy, E.; Windisch, S.; Stosick, A. J.; Hoffman, J. R. *Trans. Metall. Soc. AIME* **1967**, 239, 1247.

<sup>50</sup> Henkelman, G.; Jónsson, H. A climbing image nudged elastic band method for finding saddle points and minimum energy paths, *J. Chem. Phys.* **2000**, *113*, 9901-9904.

<sup>51</sup> Henkelman, G.; Jónsson, H. Improved Tangent Estimate in the Nudged Elastic Band Method for Finding Minimum Energy Paths and Saddle Points, *J. Chem. Phys.* **2000**, *113*, 9978-9985.

<sup>52</sup> Bader, R. F. W. *Atoms in Molecules: A Quantum Theory*; Oxford University Press: New York, 1990.

- 1  
2  
3  
4 53 Tang, W.; Sanville, E.; Henkelman, G. A grid-based Bader analysis algorithm without lattice  
5 bias. *J. Phys.: Condens. Matter.* **2009**, *21*, 084204 (7 Pages).  
6  
7  
8  
9 54 Becke, A. D.; Edgecombe, K. E. A simple measure of electron localization in atomic and  
10 molecular systems. *J. Chem. Phys.* **1990**, *92*, 5397-5403.  
11  
12  
13 55 Silvi, B.; Savin, A. Classification of chemical bonds based on topological analysis of electron  
14 localization functions. *Nature* **1994**, *371*, 683-686.  
15  
16  
17  
18 56 Wu, J.; Helveg, S.; Ullmann, S.; Peng, Z.; Bell, A.T. Growth of encapsulating carbon on  
19 supported Pt nanoparticles studied by in situ TEM. *J. Catal.* **2016**, *338*, 295-304.  
20  
21  
22  
23 57 Peng, Z.; Somodi, F.; Helveg, S.; Kisielowski, C.; Specht, P.; Bell, A.T. High-resolution in situ  
24 and ex situ TEM studies on graphene formation and growth on Pt nanoparticles, *J. catal.* **2012**,  
25 *286*, 22-29.  
26  
27  
28  
29 58 Frenkel, A. I.; Hills, C. W.; Nuzzo, R. G. A View from the Inside: Complexity in the Atomic  
30 Scale Ordering of Supported Metal Nanoparticles. *J. Phys. Chem. B* **2001**, *105*, 12689-12703.  
31  
32  
33  
34 59 Schweizer, E.; Persson, B. N. J.; Tüshaus, M.; Hoge, D.; Bradshaw, A. M. The potential  
35 energy surface, vibrational phase relaxation and the order-disorder transition in the adsorption  
36 system Pt{111}-CO. *Surf. Sci.* **1989**, *213*, 49-89.  
37  
38  
39  
40  
41 60 Kinne, M.; Fuhrmann, T.; Whelan, C. M.; Zhu, J. F.; Pantförder, J.; Probst, M.; Held, G.;  
42 Denecke, R.; Steinrück, H.-P. Kinetic parameters of CO adsorbed on Pt(111) studied by in situ  
43 high resolution x-ray photoelectron spectroscopy. *J. Chem. Phys.* **2002**, *117*, 10852-10859.  
44  
45  
46  
47  
48 61 Feibelman, P. J.; Hammer, B.; Nørskov, J. K.; Wagner, F.; Scheffler, M.; Stumpf, R.; Watwe,  
49 R.; Dumesic, J. The CO/Pt(111) Puzzle. *J. Phys. Chem. B* **2001**, *105*, 4018  
50  
51  
52  
53 62 Olsen, R. A.; Philipsen, P. H. T.; Baerends, E. J. CO on Pt(111): A puzzle revisited. *J. Chem.*  
54 *Phys.* **2003**, *119*, 4522-4528.  
55  
56  
57

1  
2  
3  
4 6<sup>3</sup> Perdew, J. P.; Wang, Y. Accurate and Simple Analytic Representation of the Electron Gas  
5  
6 Correlation Energy. *Phys. Rev. B: Condens. Matter Mater. Phys.* **1992**, *45*, 13244–13249.

7  
8  
9 6<sup>4</sup> Burke, K.; Perdew, J. P.; Wang, Y. In *Electronic Density Functional Theory: Recent Progress*  
10  
11 *and New Directions*; Dobson, J. F., Vignale, G., Das, M. P., Eds.; Plenum: 1998.

12  
13 6<sup>5</sup> Wang, T.; Wang, S.; Li, Y.-W.; Wang, J.; Jiao, H. Adsorption Equilibria of CO Coverage on  
14  
15  $\beta$ -Mo<sub>2</sub>C Surfaces. *J. Phys. Chem. C* **2012**, *116*, 6340–6348

16  
17  
18 6<sup>6</sup> Medford, A. J.; Vojvodic, A.; Studt, F.; Abild-Pedersen, F.; Nørskov, J. K. Elementary Steps  
19  
20 of Syngas Reactions on Mo<sub>2</sub>C(001): Adsorption Thermochemistry and Bond Dissociation. *J.*  
21  
22 *Catal.* **2012**, *290*, 108–117.

23  
24  
25 6<sup>7</sup> B. Hammer, L. Hansen, J.K. Nørskov, Improved Adsorption Energetics within Density-  
26  
27 Functional Theory Using Revised Perdew–Burke–Ernzerhof Functionals. *Phys. Rev. B* **1999**, *59*,  
28  
29 7413–7421,

30  
31  
32 6<sup>8</sup> Pistonesi, C.; Proncato, M. E.; Bugyi, L.; Juan, A. Theoretical Model for CO Adsorption and  
33  
34 Dissociation on Clean and K-Doped  $\beta$ -Mo<sub>2</sub>C Surfaces. *J. Phys. Chem. C* **2012**, *116*,  
35  
36 24573–24581

37  
38  
39 6<sup>9</sup> Garg, A.; Goncalves, D. S.; Liu, Y.; Wang, Z.; Wang, L.; Yoo, J. S.; Kolpak, A.; Rioux, R.  
40  
41 M.; Zanchet, D.; Román-Leshkov, Y. Impact of Transition Metal Carbide and Nitride Supports  
42  
43 on the Electronic Structure of Thin Platinum Overlayers. *ACS Catal.* **2019**, *9*, 7090-7098

44  
45  
46 7<sup>0</sup> Luo, Y.-R. *Comprehensive Handbook of Chemical Bond Energies*; CRC Press, Taylor and  
47  
48 Francis Group: Boca Raton, FL, **2007**.

49  
50  
51 7<sup>1</sup> Gutsev, G. L.; Bartlett, R. J.; Compton, R. N. A Electron affinities of CO<sub>2</sub>, OCS, and CS<sub>2</sub>. *J.*  
52  
53 *Chem. Phys.* **1998**, *108*, 6756-6762.

- 1  
2  
3  
4 72 McNeill, A. S.; Dixon, D. A. Energetics of CO<sub>2</sub><sup>-</sup> in Aqueous Solution. *J. Phys. Chem. A* **2019**,  
5  
6  
7 123, 1243–1259
- 8  
9 73 Purvis, G. D., III; Bartlett, R. J. A Full Coupled Cluster Singles and Doubles Model: The  
10  
11 Inclusion of Disconnected Triples. *J. Chem. Phys.* **1982**, 76, 1910–1918.
- 12  
13 74 Raghavachari, K.; Trucks, G. W.; Pople, J. A.; Head-Gordon, M. A Fifth-Order Perturbation  
14  
15 Comparison of Electron Correlation Theories. *Chem. Phys. Lett.* **1989**, 157, 479–483.
- 16  
17 75 Pople, J. A.; Binkley, J. S.; Seeger, R. Theoretical Models Incorporating Electron Correlation.  
18  
19 *Int. J. Quantum Chem.* 1976, 10, 1–19.
- 20  
21 76 Møller, C.; Plesset, M. S. Note on an Approximation Treatment for Many-Electron Systems.  
22  
23 *Phys. Rev.* 1934, 46, 618–622.
- 24  
25 77 Hwu, H. H.; Chen, J. G. Surface Chemistry of Transition Metal Carbides. *Chem. Rev.* **2005**,  
26  
27 105, 185–212
- 28  
29 78 Steinfeld, J. I.; Francisco, J. S.; Hase, W. L. Chemical Kinetic and Dynamics, 2nd ed.; Prentice  
30  
31 Hall: Englewood Cliffs, NJ, 1999.
- 32  
33 79 Ni, L.; Kuroda, K.; Zhou, L. P.; Kizuka, T.; Ohta, K.; Matsuishi, K.; Nakamura. Kinetic Study  
34  
35 of Carbon Nanotube Synthesis over Mo/Co/MgO catalysts. *J. Carbon* **2006**, 44, 2265–2272.
- 36  
37 80 Tominaga, H.; Nagai, M. Density Functional Theory of Water-Gas Shift Reaction on  
38  
39 Molybdenum Carbide. *J. Phys. Chem. B*, **2005**, 109, 20415–20423.
- 40  
41 81 Smith R. J. B.; Loganathany, M.; Shantha, M. S. A Review of the Water Gas Shift Reaction  
42  
43 Kinetics. *Int. J. Chem. React. Eng.* **2010**, 8, Review R4.
- 44  
45 82 Kattel, S.; Yan, B. H.; Chen, J. G. G.; Liu, P. CO<sub>2</sub> Hydrogenation on Pt, Pt/SiO<sub>2</sub> and Pt/TiO<sub>2</sub>:  
46  
47 Importance of Synergy Between Pt and Oxide Support. *J. Catal.* **2016**, 343, 115–126.
- 48  
49  
50  
51  
52  
53  
54  
55  
56  
57  
58  
59  
60

1  
2  
3  
4 <sup>83</sup> Gao, J.; Liu, Q.; Gu, F.; Liu, B.; Zhong, Z.; Su, F. Recent Advances in Methanation Catalysts  
5 for the Production of Synthetic Natural Gas. *RSC Adv.* **2015**, *5*, 22759–22776.  
6

7  
8  
9 <sup>84</sup> Trimm, D. Coke Formation and Minimisation During Steam Reforming Reactions. *Catal.*  
10 *Today* **1997**, *37*, 233 -238.  
11

12  
13 <sup>85</sup> Kogler, M.; Köck, E. M.; Klötzer, B.; Schachinger, T.; Wallisch, W.; Henn, R.; Huck, C. W.;  
14 Hejny, C.; Penner, S. High-Temperature Carbon Deposition on Oxide Surfaces by CO  
15 Disproportionation. *J. Phys. Chem. C* **2016**, *120*, 1795–1807.  
16  
17  
18  
19  
20  
21  
22  
23  
24  
25  
26  
27  
28  
29  
30  
31  
32  
33  
34  
35  
36  
37  
38  
39  
40  
41  
42  
43  
44  
45  
46  
47  
48  
49  
50  
51  
52  
53  
54  
55  
56  
57  
58  
59  
60

## TOC

